HIGH PERFORMANCE MICROCHANNEL HEAT EXCHANGER DESIGN

By

RYAN GRIFFIN

A thesis submitted in partial fulfillment of
the requirements for the degree of

MASTER OF SCIENCE IN MECHANICAL ENGINEERING

WASHINGTON STATE UNIVERSITY
School of Mechanical and Materials Engineering

DECEMBER 2023

To the Faculty of Washington State University:

The members of the Committee appointed to examine the thesis of RYAN GRIFFIN find it satisfactory and recommend that it be accepted.

_____
Dustin McLarty, Ph.D., Chair

_____
Arda Gozen, Ph.D.

_____
Konstantin Matveev, Ph.D.

ACKNOWLEGMENT

I would like to thank my friends and family for their love, motivation, and encouragement throughout my academic career. I would also like to thank my advisors, instructors, and colleagues for their support and guidance towards helping me achieve my goals.

HIGH PERFORMANCE MICROCHANNEL HEAT EXCHANGER DESIGN

Abstract

by Ryan Griffin, M.S.
Washington State University
December 2023

Chair: Dustin McLarty

Novel manufacturing methods allows for miniaturization of microchannel dimensions with the potential to enhance heat exchanger performance by increasing surface area per unit mass. In this thesis, microchannel heat exchanger design is analyzed to determine factors limiting effectiveness and power density. Ideal heat exchanger performance is characterized for one-pass counterflow heat exchangers with varying channel dimensions, flow regimes, and thermal conductivities. Smaller channel sizes lead to increased pressure drop and temperature gradients within the channel, necessitating low flow rates. Axial conduction is found to drive down effectiveness at low flow rates, with this effect more pronounced with decreased channel dimensions. Reducing the heat exchanger's thermal conductivity to $1\frac{\mathrm{W}}{\mathrm{m}\cdot\mathrm{K}}$ is found to reduce axial conduction. However, pressure drop still limits performance for existing designs, so optimized designs are necessary to create high performance microchannel heat exchangers. A multi-pass design consisting of stacked one-pass layers to keep pressure drop at an acceptable level is tested at various channel dimensions and flow regimes. The multi-pass design achieved an 11.2 times

increase in power density and 1.08 times increase in maximum achievable effectiveness over leading commercial heat exchanger designs.

TABLE OF CONTENTS

Page

LIST OF TABLES

Page

LIST OF FIGURES

CHAPTER ONE: INTRODUCTION

The Clean Energy Systems Integration (CESI) lab is testing dry-powder additive manufacturing at the 10-200 micron scale. Co-deposition of fugitive material creates microchannels within a fully dense ceramic structure. This method could manufacture high performance microchannel heat exchangers with intricate flow patterns and geometries optimized for high effectiveness and power density. **Figure 1** shows a prototype dry-powder additive manufacturing device with ceramic nanopowder deposited on the plunger of the press, while **Figure 2** displays an example of a sub-100 µm contagious channel produced using this method.

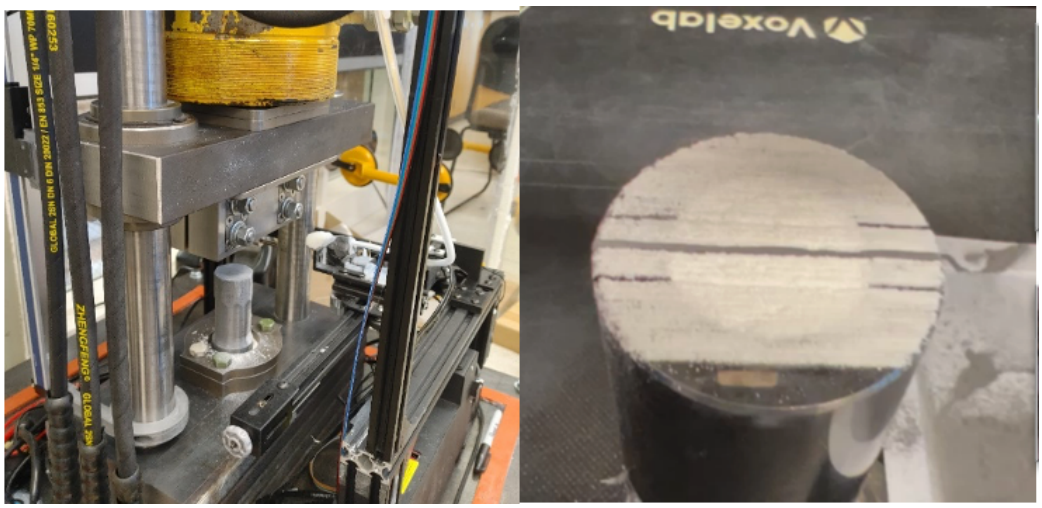

Figure 1 Dry-Powder Additive Manufacturing Using Ceramic Nanopowder

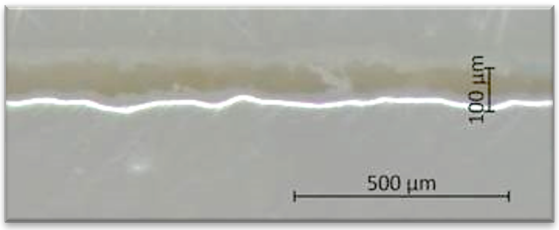

Figure 2 Dry Sub-100 μm Microchannel

For a constant length heat exchanger, reducing channel dimensions leads to an increase in power density by increasing the surface area to volume ratio [1,2]. However, this advantage diminishes with increasing length. This justifies the development of finer manufacturing techniques to reduce channel dimensions and increase power density. When manufacturing reaches the microscale (50-500 μm), axial conduction limits effectiveness. Further miniaturization of channel dimensions is impractical without changes in design or material.

Ceramic microchannel heat exchangers have the potential to outperform their metal counterparts due to the lower thermal conductivity of ceramics. Lowering the thermal conductivity reduces the influence of axial conduction, leading to a higher effectiveness heat exchanger [3,4]. However, lowering the thermal conductivity of the material does not always lead to improved effectiveness, as it can also limits heat transfer between the hot and cold fluids. This novel manufacturing process allows for design optimization to maximize ceramic microchannel heat exchanger performance.

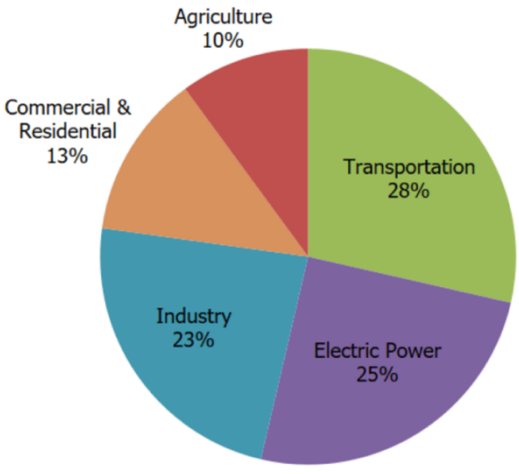

Figure 3 US Greenhouse Gas Emission by Economic Sector [5]

Solid oxide cells (SOCs) are one possible application that can utilize a high performance heat exchanger. The transportation sector is the single largest contributor to greenhouse gas emissions in the United States, accounting for 28% of the nation's carbon emissions, as shown in **Figure 3**. This provides a major need for renewable energy in transportation to reduce carbon emissions, and solid oxide fuel cells (SOFCs) are a promising potential candidate due to their low emissions and high efficiency. However, to provide a competitive alternative to combustion engines, SOFCs must be compact, lightweight, and highly efficient. To achieve high efficiency, heat exchangers often accompany SOCs to transfer the thermal energy in the exhaust gases to the incoming fuel. However, if a heat exchanger is used with an SOC, especially for transportation purposes, it needs to have both a high effectiveness and high power density to efficiently transfer heat in a compact and weight-conscious manner [6].

SCOPE OF WORK

The goal of this work is to analyze microchannel heat exchanger design to determine factors limiting effectiveness and power density. Novel manufacturing methods allows for miniaturization of microchannel dimensions unlocking the potential to enhance heat exchanger performance in potential applications, such as when integrated with SOCs. Chapter Two explores several factors that impact effectiveness or power density, including flow regime, channel geometry, pressure drop, axial conduction, thermal conductivity of the heat exchanger material, and fluid properties. It also contains background information pertaining to SOC conditions and

requirements for accompanying heat exchangers. A literature review is conducted for ceramic and metal microchannel heat exchangers.

Chapter Three discusses the computational fluid dynamics (CFD) software in detail and how it is used to test heat exchanger performance. CFD simulations are separated into three categories based on their independent variable, including variations in channel dimensions, flow regime, and thermal conductivity of the heat exchanger material. The NTU method is used to determine length scales based on given channel geometry and fluid properties, while deviations in expected performance from NTU are discussed. Specific geometry, operating conditions, and CFD settings pertaining to all simulations are specified with an emphasis on testing the ideal performance of the heat exchanger under SOC conditions.

Chapter Four presents a quantitative comparison of heat exchanger performance across different length scales and flow domains, including variations in Reynold's number. CFD computes the pressure drop as an important design criterion that can limit performance. A Reynold's number study investigates axial conduction's impact limiting peak effectiveness. The final set of simulations lowers the thermal conductivity of the heat exchanger material, using nickel, alumina, 8YSZ, and glass in place of copper. Despite reducing axial conduction and raising the effectiveness at low flow rates, the effectiveness of one-pass heat exchangers using conventional designs are limited in acceptable length dictated by the allowable pressure drop, necessitating design changes.

Chapter Five looks to solve the issue of pressure drop limiting effectiveness by using an optimized multi-pass system design, with one-pass layers stacked on top one another, resulting in low pressure drop in each layer due to the short length. This allows for higher flow rates to be used to increase effectiveness and power density. The multi-pass system models are examined and discussed, along with potential downsides compared to a one-pass heat exchanger. Similar to Chapter Four, CFD simulations are run at the same conditions to compare multi-pass to one-pass performance for varying channel dimensions and flow rates. This system provides greater flexibility and meets the goals for a heat exchanger with both high effectiveness and power density.

CHAPTER TWO: BACKGROUND

One of the most common metrics to quantitatively describe heat exchanger performance is effectiveness. Effectiveness is defined as the ratio between the actual amount of heat transferred to the maximum possible heat transfer between two fluids. For two heat exchangers with constant conditions, one with a higher effectiveness value means that it can transfer the same amount of heat with less energy. Therefore, a high effectiveness heat exchanger is desirable because it transfer heat efficiently with minimal surface area, reducing weight and cost to manufacture.

The other desirable metric for a heat exchanger used along with SOFC and SOEC applications is power density. Thermal power density is defined as the amount of heat transferred per unit volume. A high power density is desirable because it implies that the heat exchanger can transfer a large amount of heat relative to its weight. This is especially important for transportation applications where weight is often minimized for improved efficiency.

There are several variables that impact effectiveness and power density that need to be optimized to get the most out of the heat exchanger performance. Flow regime, geometry, axial conduction, material thermal conductivity, fluid properties, and pressure drop can all be optimized to achieve the highest possible effectiveness and power density.

A counterflow flow pattern is often used over cross flow or parallel flow because of the greater temperature difference between the fluids, allowing for greater heat transfer [7].

Additionally, a counterflow pattern reduces the thermal stress imposed on the walls of the heat exchanger by minimizing the temperature gradient across the walls of the channels. Turbulent flow results in higher heat transfer due to the increased fluid mixing but laminar flow is often used reduce the pressure drop across the heat exchanger. Harms found a Reynold's number less than 1600 is ideal for copper microchannel heat exchangers with rectangular channels [8]. Lewinsoh analyzed ceramic microchannel heat exchangers and found a Reynold's number of 500-600 was ideal to minimize pressure drop while still having adequate heat transfer. The study concludes that channel geometries should be optimized to fit this flow regime [9].

Flow regime and channel geometry are closely linked in their impact on heat exchanger performance. To maximize heat transfer, the surface area the two fluids are in contact should be maximized to allow more room to exchange heat. Therefore, smaller channel sizes have a higher surface area to volume ratio, promoting heat transfer and leading to a higher effectiveness. Hasan et. al. found that square channels provide the second best performance based on effectiveness and heat transfer behind circular shaped channels for a counterflow microchannel heat exchanger at a Reynold's number of 50. Other shapes tested included triangle, trapezoid, and rectangular channels [10]. Muzychka found that square and triangular shaped microchannels provide the most heat transfer per volume [11]. Kumar et. al. determined rectangular channels outperformed square channels in the size range of 0.2 mm to 1 mm [12]. Vontas et. al. found that there exists an optimal hydraulic diameter for microchannel heat exchangers that maximizes heat flux [13].

While maximizing the surface area to volume ratio leads to greater heat transfer, it also leads to a high pressure drop across the heat exchanger. Pressure drop is defined as the loss of

pressure as the fluid moves along the length of the heat exchanger. This leads to a pressure gradient between the inlet and outlet of the fluid channel. It is caused by the viscous effects as the fluid interacts with the wall and within the fluid, causing velocity and energy dissipation, resulting in loss of fluid pressure. A high pressure drop causes structural issues for the heat exchanger as the material needs to handle the pressure gradient. It can also lead to decreased heat exchanger performance due to its impact on flow rate, which can affect heat transfer rates both in the fluid and between both fluid streams.

For laminar, steady, fully developed flow in a square channel, pressure drop is characterized using the Hagen-Poiseuille equation shown in **Equation 1**. Therefore, pressure drop is proportional to both length of the heat exchanger and flow rate, while it is inversely proportional to the square of the cross sectional area of the channel [14].

$$\Delta P = \frac{8\pi\mu LQ}{A^2} \tag{1}$$

Another issue that can arise when flow channel dimensions decrease is axial conduction. Axial conduction is transfer of heat along the length of the heat exchanger through the solid material. For a counterflow heat exchanger, there is a temperature gradient that occurs between the hot fluid inlet and the cold fluid inlet. This large temperature gradient drives heat transfer along the length of the heat exchanger. Axial conduction hurts heat exchanger performance by decreasing the temperature gradient across the membrane separating the fluids, reducing heat transfer. There are three instigating factors that influence axial conduction including fluid properties including fluid properties that impact the thermal boundary layer, solid material

properties that dictate conductive heat transfer, and the geometry of the channels relative to the walls and membrane.

A thinner thermal boundary layer can result in higher rates of heat transfer between the solid material and the fluid flowing through the channels. Therefore, fluid properties such as viscosity and thermal conductivity that influence the size of the thermal boundary layer also impact the rates of axial conduction. Another method to limit axial conduction is to limit heat transfer through the solid material, accomplished by lowering the material thermal conductivity. Finally, axial conduction increases as the size of the channel relative to the wall and membrane thickness decreases.

Axial conduction also can occur through the walls of the fluid channels. The walls are in constant contact with both the hot and cold fluid, so heat is constantly being transferred. Since the walls of the channels are in contact with the membrane separating the fluids, the heat is then transferred into the membrane. This leads to higher rates of axial conduction as more heat moves through the membrane along the direction of flow. While this effect can often be negligible when wall thickness is much smaller than channel size, this effect can be significant for microchannels where the channel size closely matches wall thickness. Other ways to reduce this phenomenon include decreasing the thermal conductivity of the walls, decreasing the temperature gradient between the fluids, decreasing wall thickness, increasing wall height, or decreasing the surface area the wall contacts the fluid.

One of the primary methods used to limit axial conduction is through lowering the thermal conductivity of the heat exchanger material. Doing so limits the heat transfer through the membrane along the fluid direction, but it can also limit heat transfer through the membrane. Maranzana et. al. proposed that there exists an optimal thermal conductivity of the solid material that maximizes efficiency by limiting axial conduction. For a counterflow microchannel heat exchanger, stainless steel outperformed copper as the solid material due to its limitation of axial conduction [15]. Lewinsohn found that lowering thermal conductivity from metal to ceramic improved effectiveness by reducing axial conduction in the walls [9]. However, the ideal thermal conductivity will vary depending on geometry, as the reduction of axial conduction and promotion of heat transfer through the membrane are balanced.

Just as the thermal conductivity of the solid material influences heat exchanger performance, so too does the thermal conductivity of the working fluid. Since SOCs utilize several different fuel gases during normal operation, the accompanying heat exchanger's performance depends on the fluid properties of the fuel used. **Table 1** highlights how the thermal conductivity and viscosity of the fluid varies for common SOC fuel gases [16]. Hydrogen gas has a significantly higher thermal conductivity than methane gas, oxygen gas, and air. This property of hydrogen gas leads to improved performance of the heat exchanger due to higher rates of heat transfer. Methane gas and hydrogen gas also have lower viscosity than oxygen gas or air, which can reduce the pressure drop across the heat exchanger.

Table 1 SOC Gas Properties at 300 K [17,18]

Gases	**Thermal Conductivity [$\frac{W}{m \cdot K}$]**	**Viscosity [μPa · s]**
H_2	0.1866	8.90
CH_4	0.0344	11.1
O_2	0.0265	20.7
Air	0.0264	18.5

To be an ideal candidate for use with SOCs, a heat exchanger needs to have certain characteristics to allow it to withstand the harsh operating conditions. SOCs typically operate between 700 and 1000℃ and between 1 and 10 bar pressure [19,20]. In addition, heat exchanger needs to be durable enough to ensure high performance throughout the long lifetime of SOC operation [21,22]. Material selection is a key factor in determining the heat exchanger's durability. The material should be chemically stable to prevent reactions from occurring with the reactant gases and to avoid contaminating the high-purity gases [23]. Limiting reactions also prevents deposits of material from forming inside the heat exchanger that can lower performance. To prevent declines in mechanical strength caused by the high temperatures and reactant gases, the materials must also be corrosion resistant [24,25]. In addition to the durability requirement, the material selection process must account for compatibility with SOC materials, including the prevention of reactions forming at the interface between the two systems.

LITERATURE REVIEW

Comparing simulated performance to experimental data, Williams et. al. found manufacturing inconsistencies in the microchannels led to performance deviations from expected results. While microchannel heat exchangers are desirable for aerospace applications due to their weight and volume requirements, manufacturing inconsistencies need to be improved upon before implementation [26]. Similarly, Mei et. al. found experimental performance of copper and aluminum microchannels differed due to a higher surface roughness than anticipated as a result of the manufacturing process. This led to increased heat transfer mixing but also higher pressure drop [27]. Khan et. al. varied the heat exchanger material to change its thermal conductivity and found that lowering thermal conductivity resulted in increased effectiveness. However, they found that the change in the material's surface roughness also significantly contributed to the performance [28].

To combat the constant issue of pressure drop, several studies have been conducted by stacking one-pass layers on top of one another, shortening the length of each channel to limit pressure drop. Kee et. al. found that stacking one-pass layers for a ceramic counterflow heat exchanger led to decreased pressure loss. The decreased pressure drop of each layer allowed for the system to reach higher effectiveness than one-pass systems [29]. Alm et. al. compared simulated results to experimental results for a stacked microchannel heat exchanger. The experimental results varied from simulated results due to manufacturing inconsistences when joini65eng layers, leading to an increased pressure drop and increased heat transfer rate than expected [30]. Kaur et. al. determined that stacking layers led to increased pressure drop due to

uneven flow distribution within the parallel channels [31,32]. Including an external manifold for gas routing helps to mitigate the issue and led to decreased pressure drop [33].

CHAPTER THREE: METHODS

Computational fluid dynamics are employed to simulate heat exchanger performance, enabling optimization based on SOC operating conditions. The three key parameters CFD will address are heat exchanger channel geometry, flow regime, and thermal conductivity of the heat exchanger material. The influence of flow channel geometry on effectiveness and power density are found by scaling the size of square fluid channels at various length scales. Next, a parametric sweep of Reynold's number is conducted to capture the critical domains where axial conduction is limited, effectiveness is maximized, and where the boundary layer temperature gradient limits the heat transfer possible. A final sensitivity study investigates the impact of material thermal conductivity.

SolidWorks Flow Simulation is chosen as the computational fluid dynamics software for this paper. It solves the Navier-Stokes equations based on the energy, mass, and momentum conservation equations [34]. It assumes all fluids are continuous and utilizes the thermophysical properties and state equations for the fluids to create a dependency for the fluid's density, viscosity, and thermal conductivity as a function of temperature. When dealing with turbulent flow, the software solves the Favre-averaged Navier-Stokes. In addition, *SolidWorks Flow Simulation* solves conjugate heat transfer problems using the energy conservation equation to describe the heat conduction through solid media [35].

The CFD simulations make several assumptions that are applied to all models tested. The simulations contain both laminar and turbulent flow with no phase change in the fluid. It neglects

humidity and assumes the Mach number is low. All wall conditions are treated as no-slip boundary conditions with no fouling considered. *SolidWorks Flow Simulation* only considers radiation between solid surfaces and does not account for radiation between solid surfaces and the environment. The simulations run until steady state is achieved and all goals are converged.

The effectiveness is found using **Equation 2**.

$$\varepsilon = \frac{\dot{m}_C c_{p,C}(T_{C,o} - T_{C,i})}{\dot{m}_H c_{p,H}(T_{H,i} - T_{C,i})} \tag{2}$$

The equation can be simplified in the case of a counterflow heat exchanger with a constant heat transfer coefficient to a comparison of enthalpy as shown in **Equation 3**.

$$\varepsilon = \frac{\dot{m}_C(h_{C,o} - h_{C,i})}{\dot{m}_H(h_{H,i} - \dot{m}_C h_{C,i})} \tag{3}$$

For a heat exchanger with balanced flow rates between the cold and hot fluid, effectiveness can then be found using only enthalpies rates, as shown in **Equation 4**.

$$\varepsilon = \frac{\dot{h}_{C,o} - \dot{h}_{C,i}}{\dot{h}_{H,i} - \dot{h}_{C,i}} \tag{4}$$

Similar to effectiveness, power density can be defined using enthalpy rates of the two fluids, as shown in **Equation 5**.

$$P = \frac{\dot{m}_C\left(h_{C,i} - h_{C,i}\right)}{V \cdot \rho} = \frac{\dot{h}_{C,o} - \dot{h}_{C,i}}{V \cdot \rho} \quad (5)$$

The CFD simulations are designed to test the ideal performance of the heat exchanger with no heat lost to the environment. The outer walls of the heat exchanger are insulated with an ideal insulator having a thermal conductivity of zero, as displayed in **Figure 4**. This leaves only the channel walls and membrane separating the fluid being composed of the heat exchanger material. An adiabatic outer wall condition is also applied to ensure no heat leaves the system. External radiative heat transfer is neglected as its effects are assumed to be minimal since the heat exchanger is surrounded by insulation.

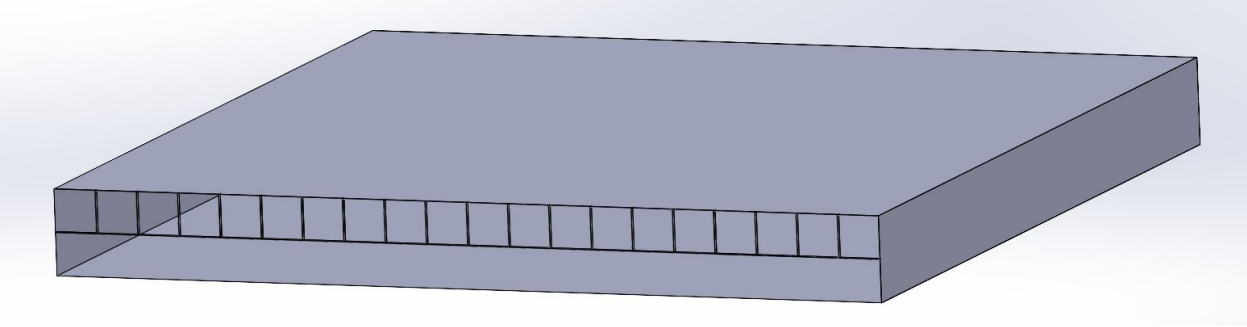

Figure 4 Surrounding Insulation for 5 mm Channel Size Heat Exchanger at Length 0.5 m with a Thickness of 0.025 mm; Inlet Lids Fit into Individual Channels to Control Inlet Mass Flow Rate; Exit Lids Span All 20 Channels and Set Exit Pressure; Location of Exit and Inlet Lids Reversed for Opposite Side

All heat exchanger models are counterflow and contain 20 square microchannels in each fluid direction, as seen in **Figure 5**. Square microchannels can be manufactured using the dry-powder additive manufacturing process. They provide high active area, allowing for increased surface area for heat transfer. Additionally, square channels minimize the heat transfer thickness of the membrane separating the two fluids, and thus minimizes the thermal resistance. The

membrane and wall thickness is held constant at 25 μm as that nears the limit of manufacturing capability. It also represents a feasible manufacturing limit due to the difficulty of fabricating such sizable channels, up to 5 mm, in comparison to their thickness. Having thin walls and membrane also facilitates heat transfer and decreases axial conduction [36]. A downside of thin walls and membrane is the risk of structural failure coming from pressure drop or thermal stress. The walls and membrane also have zero surface roughness to promote a uniform flow distribution.

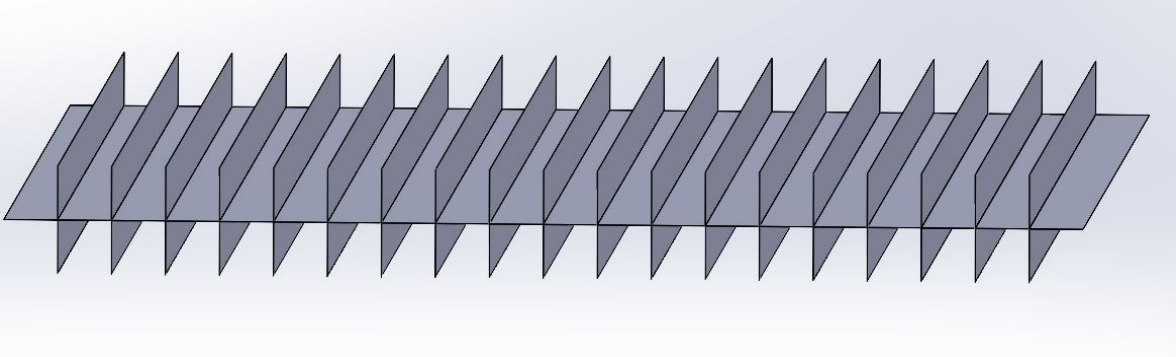

Figure 5 Walls and Membrane for 20 Square Channels at 5 mm in Size with Constant Wall and Membrane Thickness of 0.025 mm

The options for boundary conditions include flow openings, pressure openings, and wall conditions. Flow openings allow for mass transfer into and out of the control volume, while pressure openings allow for pressure conditions within the fluid, the environment, or total pressure. Wall conditions can be assigned to designate material as an ideal or real wall. Mass flow rates are chosen at the inlets of the heat exchanger to ensure even flow distribution at a specific Reynold's number. For the outlets, an environmental pressure is applied, allowing the pressure drop across the heat exchanger to be determined.

Lids are required at all fluid inlets and outlets to fully define the fluid volume for internal flow, so all boundary conditions are applied to the inlet and outlet lids. Separate inlet lids are created for each channel to control the Reynold's number in each channel. A single outlet lid assigning a uniform outlet pressure spans across all the channels. The goals for the simulation are determined based on the average fluid properties of the lids. Since the number of inlet lids varies with the number of channels, their fluid properties are averaged to get an overall evaluation of the fluid at the inlets. The simulations determine the enthalpy rate at both the inlet and outlet lids for both fluids.

Several operating conditions are held constant across all models. The working fluid for both streams is air, with the hot inlet set at 815℃ and the cold inlet at 20℃. The fluid flow rates are balanced, have a uniform profile, and are not fully developed. Both laminar and turbulent flows are considered with the turbulence intensity set to 2% and the turbulence length at 0.02 mm. The exit pressure is held constant at 10 bar. The initial solid temperature is set to 20℃ for one-pass systems and 815℃ for multi-pass systems.

Finally, the models have a global mesh with at least three cells across each fluid channel. Along the fluid direction, at least 400 cells are used to capture the temperature change of the fluid as it moves along the heat exchanger. Due to the thin thickness of the walls and membrane, a local mesh is applied to assure that each solid boundary has at least three cells. The exact number of cells depends on the channel geometry and length of the model.

Length scales for the models are determined based on theoretical effectiveness found using numerical modeling, based on **Equation 6**.

$$\varepsilon = \frac{1 - e^{-NTU(1-R)}}{1 - Re^{-NTU(1-R)}} \tag{6}$$

The ratio of thermal capacity is found using **Equation 7**.

$$R = \frac{C_{min}}{C_{max}} = \frac{\dot{m}c_{p,C}}{\dot{m}c_{p,H}} \tag{7}$$

In the CFD models, the mass flow rates of the cold and hot fluid are equal, creating balanced flow. This further simplifies **Equation 7**. NTU can then be found using **Equation 8.**

$$NTU = \frac{UA}{\dot{m}C_{min}} \tag{8}$$

The overall heat transfer coefficient is found using a relation for the total thermal resistance of the system, shown in **Equation 9**.

$$\frac{1}{U} = \frac{1}{R_{Th}} = \frac{1}{R_{Conv,H} + R_{Cond} + R_{Conv,C}} \tag{9}$$

Convective and conductive thermal resistance are defined in **Equations 10** and **11** respectively.

$$R_{Conv} = \frac{1}{h \cdot A_s} \tag{10}$$

$$R_{Cond} = \frac{L}{k \cdot A} \tag{11}$$

The final step to solve the NTU effectiveness is to find the convective heat transfer coefficient, since all other variables are known. If we assume that the flow in the channel is fully-developed, internal laminar flow, we can find a relation for the convective heat transfer coefficient using **Equation 12**.

$$Nu = \frac{h \cdot D_h}{k_{fluid}} \tag{12}$$

Assuming the flow is fully-developed internal laminar flow, yields a known Nusselt number of 3.61 for square fluid channels [37]. Knowing the Nusselt number provides a solution for the heat transfer coefficient since all other variables in **Equation 12** are known.

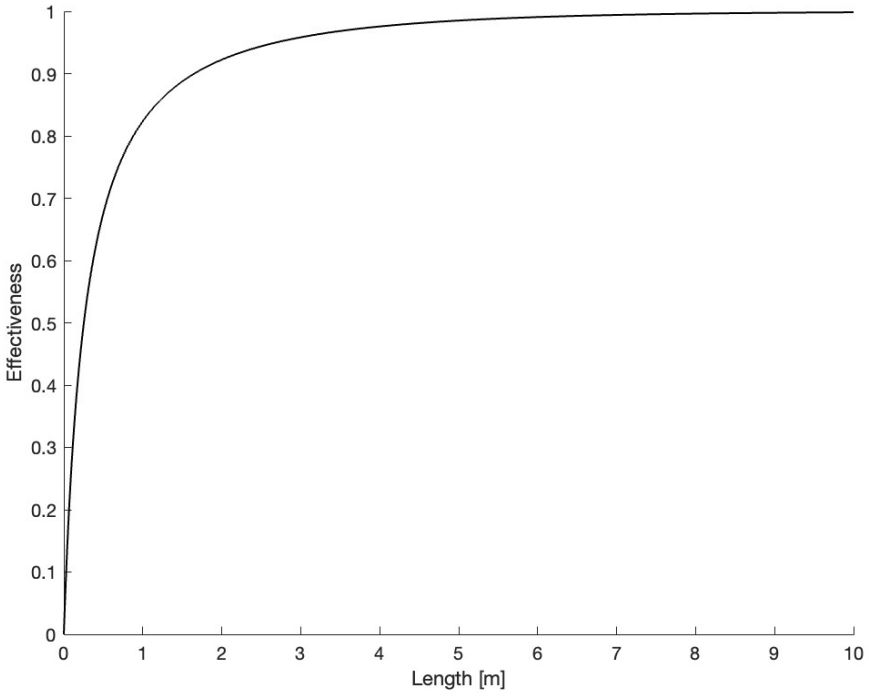

Figure 6 NTU Effectiveness for Copper Heat Exchanger with 5 mm Square Channels, Air as Fluid at 200 Re, Hot Inlet at 815℃, Cold Inlet at 20℃, and Membrane Thickness of 0.025 mm

Once the heat transfer coefficient is known, the NTU method effectiveness can be plotted as a function of length for a copper heat exchanger. **Figure 6** shows the results for a square channel with a width of 5 mm. Plotting the NTU effectiveness for smaller channel dimensions of 0.5 mm and 0.05 mm results in the same curve but with the length scale reduced by a factor of 10 and 100, respectively. Based on the results, it was determined that the length ranges for the copper heat exchanger would extend to 10 meters for the 5 mm channel dimensions, 1 meter for the 0.5 mm dimension, 0.1 meters for the smallest dimension of 0.05 mm. These ranges capture both the extended length regions were the heat exchanger reaches an effectiveness close to one and the shorter length regions where the decreased mass can yield high power density.

To justify the increased length of the heat exchanger for the larger channel dimensions, consider increasing the size of a channel by a factor of 10 at a constant Reynold's number. This decreases the cross-sectional area by 100 times, resulting in 10 times lower mass flow rate. As you increase the channel dimensions by factor of 10, Nusselt number decreases by an equivalent amount due to lower heat transfer surface area. Maintaining the same heat transfer rate thus requires 100 times the volume, necessitating the increase in length scale by a factor of 10.

However, the assumptions the NTU method uses to predict effectiveness will result in deviations of simulation results from **Figure 6**. The NTU method makes two significant assumptions that can cause the predicted effectiveness to differ from actual performance. First, the NTU method neglects the effects of axial conduction, which reduces the temperature gradient between the fluid. Axial conduction will cause a greater deviation from NTU at shorter lengths as the length separating the cold and hot inlets are reduced. Consequently, this leads to changes in the heat transfer rate and temperature distribution of the heat exchanger. This deviation occurs regardless of channel dimensions.

The second NTU shortcoming is affected by flow channel dimensions. The NTU method assumes a constant temperature profile within a cross section of the channel. In reality, a temperature gradient exists due to insufficient heat transfer and mixing. The presence of this thermal gradient within the fluid restricts heat transfer by reducing the temperature gradient across the solid membrane. Microscale channels exasperates this boundary layer impact making NTU predictions unreliable at the manufacturing scale of interest.

Taking both NTU method shortcomings into account, the simulation effectiveness will vary from that shown in **Figure 6**. At shorter lengths, the effectiveness will be reduced due to the influence of axial conduction. At longer lengths, the effectiveness will again drop from increased temperature gradients within the fluid. This leads to a point where the effectiveness peaks after the axial conduction effects are overcome, before dropping off as the temperature gradient causes a decrease in effectiveness. This confirms Parahovnik et. al. findings that the NTU method deviates from expected due to axial conduction in the walls for a microchannel heat exchanger [38]. While there are some inaccuracies with the NTU method to determine effectiveness, it still provides a reasonable starting point to establish the length ranges for the initial simulation models.

The flow simulation models are separated into three distinct categories corresponding to each of the three goals for the CFD simulations. The first set varies flow channel geometry for a copper heat exchanger. Copper is selected as the heat exchanger material due to its common usage, high thermal conductivity, and high melting point. The square channel widths tested include 5 mm, 0.5 mm, and 0.05 mm. Similar to the 25 μm wall and membrane thickness, the smallest channel dimension is chosen based on manufacturing capabilities, with the others scaled up from there. Likewise, the largest channel dimension of 5 mm is governed by the manufacturing difficulties from having such sizable channels with relatively thin walls and

membrane. **Figure 7** shows the relative channel size compared to the wall and membrane thicknesses.

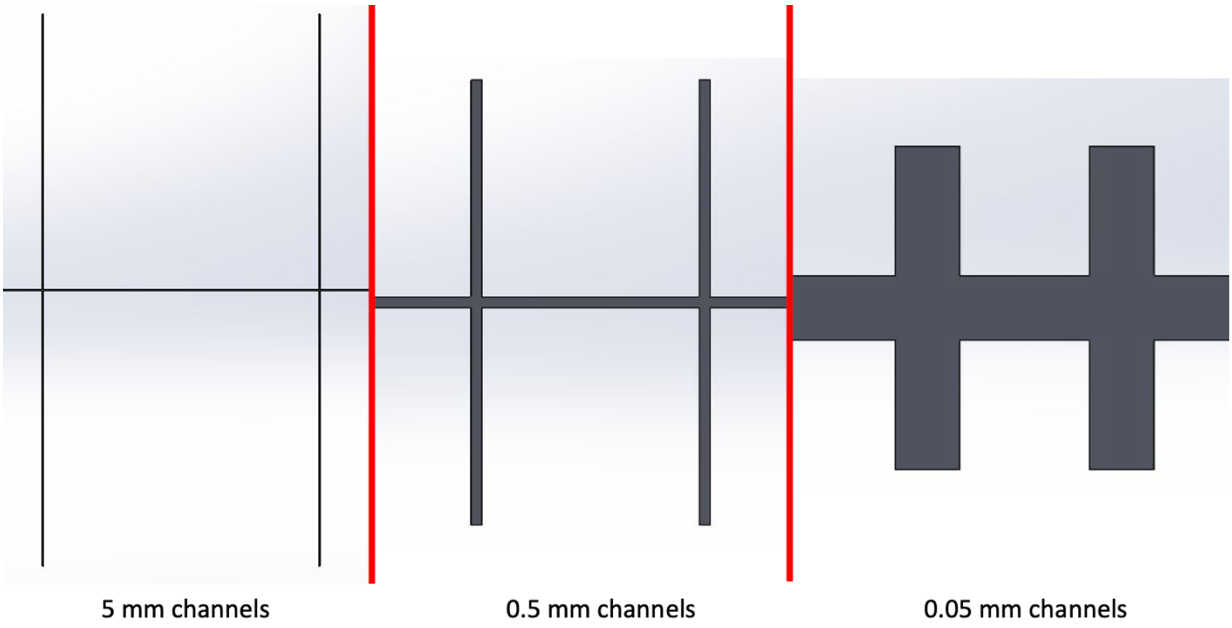

Figure 7 Comparison of Relative Wall and Membrane Thickness for Each Channel Size

To assess the influence of different channel dimensions and the general performance trend as flow rate changes, each heat exchanger model is tested at two different flow rates in the laminar region, corresponding to Reynold's values of 200 and 1000. For the 5 mm channels, the length scales tested are 0.1, 0.25, 0.5, 1, 2.5, 5, and 10 meters. The middle dimension of 0.5 mm is tested at 0.05, 0.075, 0.1, 0.25, 0.5, and 1 meters, and the final dimension of 0.05 mm is tested at 0.005, 0.0075, 0.01, 0.025, 0.05, and 0.1 meters. Extra models are tested using 5 mm channel dimensions to provide for additional comparisons of equal length heat exchangers with varying channel dimensions.

The second set of flow simulation models aims to determine the ideal flow regime for microchannels. Throughout this set, the channel dimensions are held constant at 0.05 mm with copper acting as the heat exchanger material. The flow regime is manipulated by adjusting the Reynold's number within the channels, spanning a range from 50 to 10,000. Specifically, the chosen intervals for the Reynold's numbers are 50, 100, 200, 500, 1000, 2500, 5000, and 10000. Additional data points are taking in the laminar region compared to the turbulent range because of the predicted drop in performance with increasing flow rate. The lengths tested are the same as length scale in the first set for the 0.05 mm channels.

Table 2 Material Properties to Test Various Thermal Conductivities [24]

Material	**Thermal Conductivity at 20℃ [$\frac{W}{m \cdot K}$]**	**Thermal Conductivity at 815℃. [$\frac{W}{m \cdot K}$]**	**Density [kg/m^3]**
Copper	393	345	8960
Nickel	90	74	8910
Alumina	16	16	3970
8YSZ	3.7	2.1	5978
Glass	1	2	2600

The third set of flow simulation models share the same square channel dimension of 0.05 mm as the second set but varies the thermal conductivity of the heat exchanger material. The five materials tested and their thermal conductivities at both 20℃ and 815℃ are listed in **Table 2** along with their corresponding densities. Since thermal conductivities are the primary focus of

this study, so the material's melting temperature and manufacturability is disregarded. Each thermal conductivity is predicted to have a unique ideal flow regime range, so each material is tested over the same Reynold's number interval as the second set. Finally, the length scale is adjusted and reduced to 2.5, 5, 10, 20, and 60 mm to better illustrate the performance change due to thermal conductivity.

The fourth and final set of models are multi-pass systems consisting of stacked one-pass layers at 0.5 mm and 0.05 mm channel dimensions. The multi-pass systems employ a counterflow design as both fluids start at opposite ends of the heat exchanger, while heat transfer between the fluids occurs in a cross flow pattern. Each fluid has 36 one-pass layers with two layers per pass, accomplished using an external manifold for gas routing. Flow rates are varied from a Reynold's number of 200 to 5,000 in increments of 200, 500, 1000, 2000, 3000, and 5000. Further details and illustrations of the multi-pass system will be discussed in Chapter Five.

CHAPTER FOUR: RESULTS

Figure 8 illustrates the results from the first set of models at a constant Reynold's number of 1000. As shown, decreasing the channel dimensions by a factor of 10 leads to an almost equivalent increase in power density at similar effectiveness values.

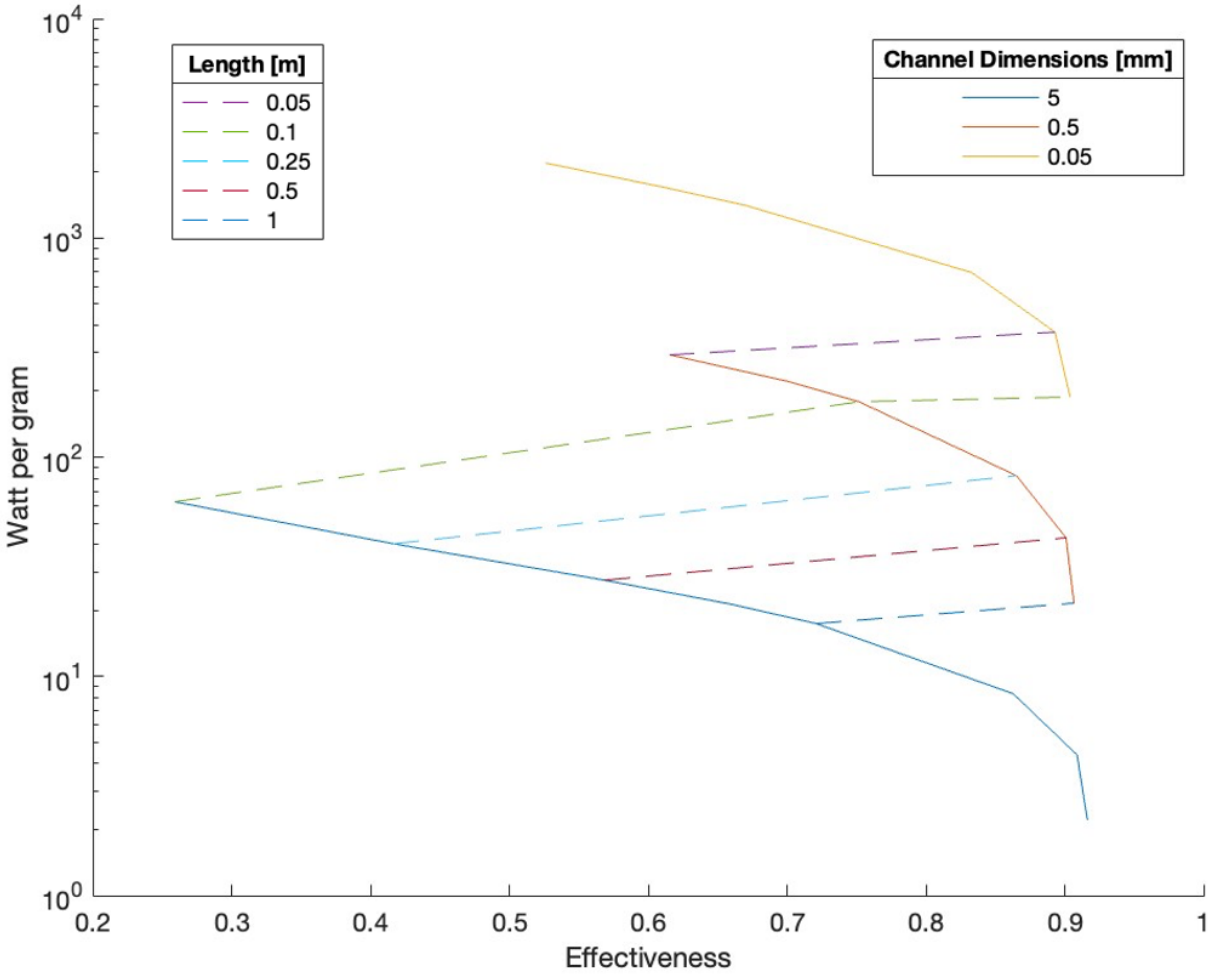

Figure 8 Copper Counterflow One-Pass Heat Exchanger with Varying Channel Dimensions for 20 Channels at a Constant Wall and Membrane Thickness of 0.025 mm; Air as the Fluid with Hot Inlet at 815°C, Cold Inlet at 20°C, and 10 Bar Exit Pressure with Flows Balanced at a Reynold's Number of 1000 in Each Channel; Insulated to Prevent Heat Loss to the Environment

However, to reach similar effectiveness values, larger channels require longer lengths, leading to a tradeoff between effectiveness and power density. Shrinking channels at a constant length comes with a significant increase in effectiveness and a slight increase in power density. This benefit is more pronounced at smaller lengths, as longer lengths experience only a slight raise in effectiveness and an almost negligible increase in power density.

Each heat exchanger design has its own effectiveness limit. As the heat exchanger approaches its maximum effectiveness, there is a substantial drop-off in power density for a small increase in effectiveness. Increasing the length does not result in considerably more heat transfer and only lowers power density as a result of the mass increase. **Figure 8** illustrates this tradeoff between effectiveness and power density that dictates design in every high performance heat exchanger application. Within the domain simulated, smaller channels always have a higher effectiveness and power density than larger channels.

The downside of using smaller channels is that the maximum effectiveness limit decreases as channel size shrinks, as seen by the rightmost extreme of each curve in **Figure 8**. At a Reynold's number of 1000 through the channels, the difference in peak effectiveness is marginal, with the difference between 5 mm and 0.05 mm channel widths being only 0.012. The decline in peak effectiveness comes from increased axial conduction, as the wall and membrane thickness increase relative to channel dimensions. However, the difference in peak effectiveness values between small and large channels should increase as flow rate decreases, since convective heat transfer diminishes, and more heat is transferred through conduction.

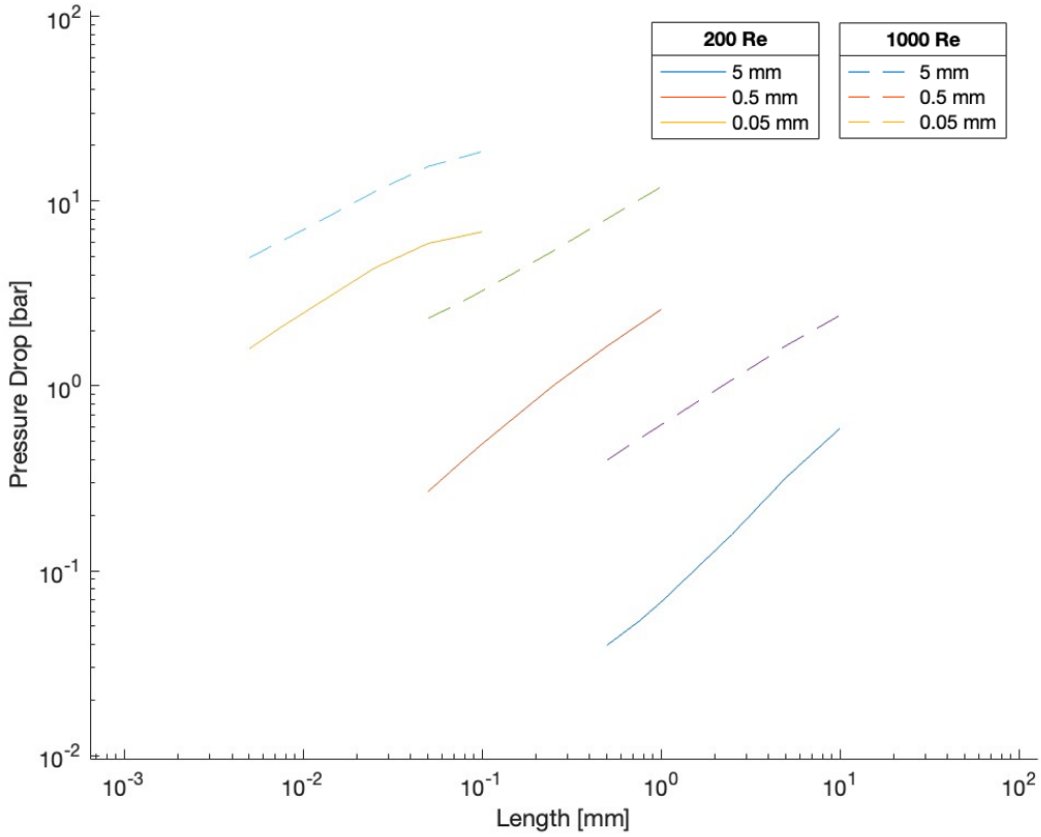

Figure 9 Pressure Drop for All Channel Dimensions Based on Equal Velocities for 0.05 mm Sized Channel at 200 and 1000 Re

Ideally, flow rate should be kept as high as possible to facilitate heat transfer and to maintain a high maximum effectiveness for small channels. The issue that arises at high flow rates is an increased pressure drop across the channel, which drops the performance of the heat exchanger. **Figure 9** displays how pressure drop worsens at higher flow rates, smaller channel dimensions, and longer lengths. To accurately compare the pressure drop across heat exchangers with different channel dimensions, equal fluid velocities were used, based on the fluid velocity in the 0.05 mm channel at a Reynold's number of both 200 and 1,000.

The smallest channel dimension always has a pressure drop greater than one bar at both 200 and 1000 Re, regardless of length. The minimum pressure drop it experiences is 1.59 bar with a maximum of 18.53 bar. Decreasing the channel dimensions by an order of magnitude allows for the pressure to drop below one bar at the low flow rate, yet the high flow rate still has a minimum of 2.32 bar. Finally, the largest channel size never extends beyond one bar for the low flow rate and only at lengths greater than 2.5 meters at the high flow rate. In addition, larger channels exhibit a greater spike in pressure drop when increasing flow rate.

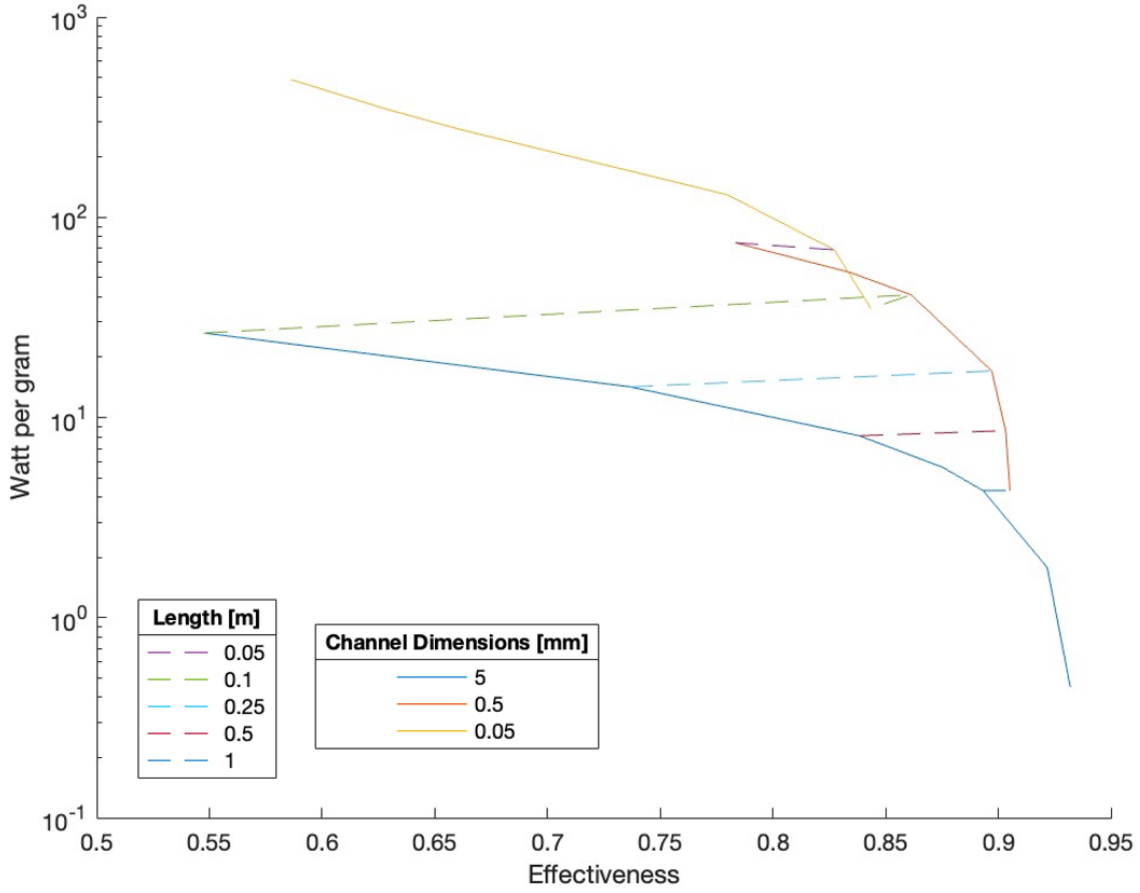

Figure 10 Copper Counterflow One-Pass Heat Exchanger with Varying Channel Dimensions for 20 Channels at a Constant Wall and Membrane Thickness of 0.025 mm; Air as the Fluid with Hot Inlet at 815°C, Cold Inlet at 20°C, and 10 Bar Exit Pressure with Flows Balanced at a Reynold's Number of 200 in Each Channel; Insulated to Prevent Heat Loss to the Environment

Since pressure drop across the heat exchanger requires low flow rates, **Figure 10** illustrates heat exchanger performance at various lengths for the three different channel dimensions with the flow rate lowered to a Reynold's number of 200. At this lower flow rate, the 5 mm channel increases its maximum effectiveness from 0.916 to 0.932 because of the decrease in pressure drop. In contrast, both the 0.5 mm and 0.05 mm show a decline in peak effectiveness due to axial conduction, with the smallest channel size experiencing the most significant drop in effectiveness from 0.904 at 1000 Re to 0.843 at 200 Re.

Reducing the flow rate causes a higher tradeoff between effectiveness and power density, as achieving an effectiveness close to one requires the heat exchanger to have large channels and a relatively low power density. Both the 0.5 mm and 0.05 mm channel dimensions have a lower power density than at 1000 Re stemming from the lower effectiveness, so reaching a high power density is harder to achieve at low flow rates. The results also show that as you scale down the channel dimensions, you experience a steeper slope of power density loss for effectiveness gain than you do with larger channels. However, the smaller channel exhibits a lesser decline in power density near the effectiveness limit.

When comparing the various channel dimensions at constant lengths, it is apparent that decreasing channel size only results in a minimal increase in power density. Therefore, it becomes challenging to raise power density at low flowrates, even by altering the channel dimensions or heat exchanger length. The cascading effects the maximum effectiveness points takes as the channel size shrink leads to a point where it is objectively better to use larger

channels because of the increase to both power density and effectiveness. This effect can be seen at 0.1 meters in length when comparing 0.5 mm and 0.05 mm channel sizes. In the same manner, decreasing from 5 mm to 0.5 mm near 1 meter in length gives a minimal increase in effectiveness and a negligible increase in power density.

Comparing **Figures 8** and **10** provides several additional insights. The first being that lower flow rates diminish the effectiveness and power density increase associated with smaller channel sizes, which can be seen by comparing the constant length lines from both plots. This effect is most noticeable near the maximum effectiveness limits at a given channel size. Additionally, there is a general decrease in power density at lower flow rates as smaller channels no longer exhibit the same level of power density at 200 Re that they did at 1000 Re. Specifically, the 0.05 mm channel size has approximately an order of magnitude decrease in power density at equal effectiveness values at a Reynold's number of 200 when compared to 1000 Re. The decreased power density results from longer lengths required to reach the same effectiveness value. At lower flow rates required by pressure drop, manufacturing smaller microchannel no longer definitively increases power density and effectiveness. In certain cases, smaller channel size leads to worse performance. Examination of the temperature profiles inside the of the flow channels sheds light on the reason for these outcomes.

Both the cross-sectional temperature profile and the temperature profile along the length of the heat exchanger are explored. The cross-sectional temperature profiles include both the solid temperature of the walls and membrane as well as the fluid temperature in the channel. The

temperature profile along the length of the heat exchanger only includes the fluid temperature of the air.

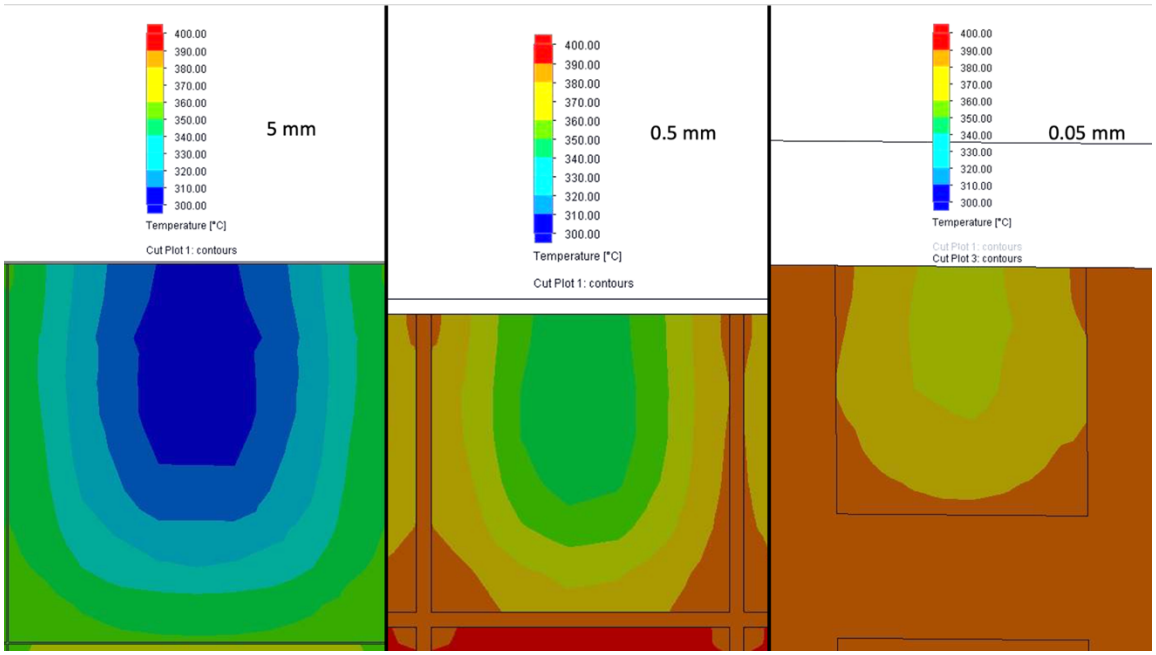

Figure 11 Cross Sectional Temperature Profile of Both Solid and Fluid Temperature

Figure 11 shows the cross-sectional temperature distribution for all three channel dimensions. Importantly, since all channels share the same Reynold's number, the velocity of the fluid inside the channel scales down by an order of magnitude as the channel dimensions scale up an equivalent amount. The increased fluid velocity in the larger channels allows for greater convective heat transfer mixing, which should yield a uniform temperature distribution. However, the smallest channel dimension has the most uniform temperature distribution of the three. Further examination of the wall and membrane temperature shows a striking similarity to the temperature distribution in the channel. Axial conduction has a stronger influence on the 0.05 mm channel since the fluid maintains a close distance to the wall as the cross-sectional area is reduced, leading to increased heat transfer between the solid and the fluid, and thus, a more

uniform temperature distribution. The larger channels are less dependent on conductive heat transfer as the relative size of the walls and membrane decrease. Therefore, axial conduction effects are more pronounced for the smallest dimension, so changing the heat exchanger material will have the largest performance influence for the smallest channels.

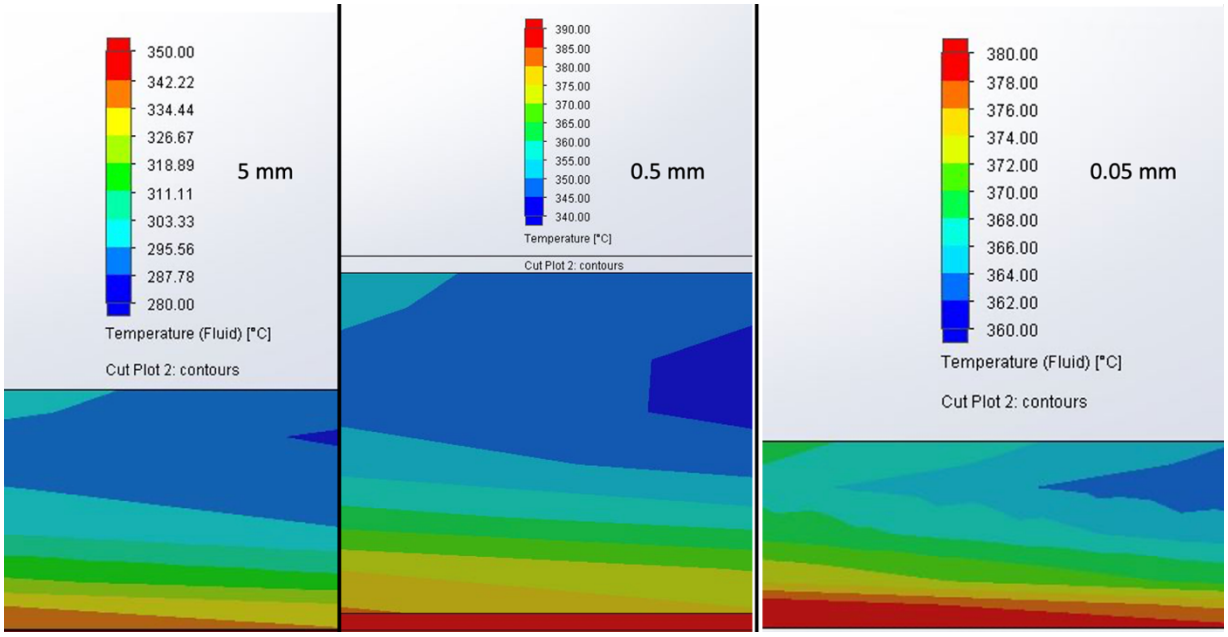

Figure 12 Temperature Profile Along the Length of the Heat Exchanger at the Midpoint of the Channel

Figure 12 displays the longitudinal temperature distribution, highlighting the rate of heat transfer away from the membrane and the temperature distribution inside the channel. Each profile is taken across the length of the heat exchanger at the midpoint of the cross section. Due to the length of the heat exchangers, the temperature profile at the midpoints are examined for the cold fluid to accurately compare all three profiles. Like the previous temperature profiles, the smallest channel dimension has the narrowest temperature distribution range. This can be partially attributed to the heat conduction through the walls being dominant for the smaller

channels, yet the relative size of the thermal boundary layer to the channel also contributes to the uniform temperature profile. For the smaller channels, the thermal boundary layer occupies a substantial portion of the fluid channel compared to the rest of the channel, allowing for higher levels of heat transfer mixing. The larger channels do not have the added advantage of utilizing the thermal boundary layer for thermal mixing since the size of the boundary layer shrinks relative to the rest of the channel. This leaves convective heat transfer as the necessary form of heat transfer to achieve a uniform temperature distribution.

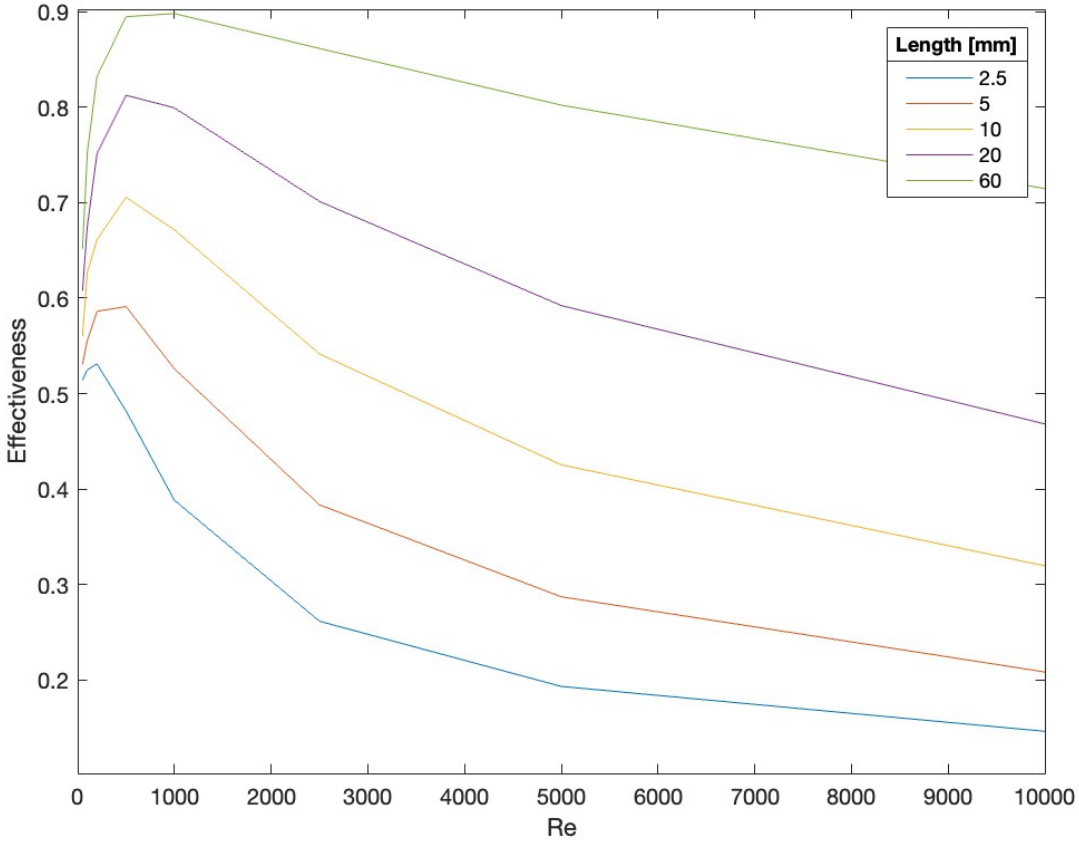

Figure 13 Copper Counterflow One-Pass Heat Exchanger with 20 Square Channels at Size 0.05 mm and a Constant Wall and Membrane Thickness of 0.025 mm; Air as the Fluid with Hot Inlet at 815℃, Cold Inlet at 20℃, and 10 Bar Exit Pressure with Flows Balanced at a Reynold's Number Ranging From 50 to 10000; Insulated to Prevent Heat Loss to the Environment

Both temperature profiles indicate that the smallest channel dimension relies on conduction as the dominant method of heat transfer. Therefore, axial conduction has an increased effect on smaller channel dimensions due to this dependence. The narrow temperature distribution range of the smaller channel sizes can potential to higher effectiveness at low flow rate if it is not limited by axial conduction. **Figure 13** shows the results of the second set of simulations where Reynold's number is varied for the 0.05 mm channel dimensions to better illustrate the effects of axial conduction.

Axial conduction's influence on performance can be seen by the low effectiveness values at the low end of the Reynold's number range. As the flow rates initially increases, there are large spikes in effectiveness as axial conduction is overcome. Across all heat exchanger lengths, the peak effectiveness occurs between a Reynold's number of 200 to 1000, with the ideal flow rate increasing as the heat exchanger length extends. Longer length heat exchangers can reach a higher peak effectiveness by reducing axial conduction, but it requires a higher flow rate.

Another benefit of the longer length is the gradual decline in effectiveness beyond that initial peak as Reynold's number increases into the turbulent flow regime. The amplified fluid velocity begins to limit heat transfer in shorter heat exchangers as there is not sufficient time for heat transfer and mixing in the fluid stream. The benefit of a more gradual decline serves no sizable benefit since the excessive length scale and high flow rate creates a significant pressure drop. At the low flow rates required by acceptable pressure loss, axial conduction limits the maximum effectiveness with copper as the heat exchanger material. Despite the long lengths

needed to reach it, the effectiveness with copper only reaches a maximum effectiveness across all lengths of 0.897 at 1000 Re.

Both the temperature distributions and the Reynold's number study indicate that axial conduction is driving down the performance of copper microchannels, negating the benefit of finer manufacturing. To mitigate this consequence, the heat exchanger material's thermal conductivity can be reduced in an effort to limit axial conduction. This approach can help to achieve the goal of a high peak effectiveness at low flow rates. The results of the final set of one-pass simulations lowers the thermal conductivity of the material and tests the performance over a range of flow rates as show in **Figures 14-17**.

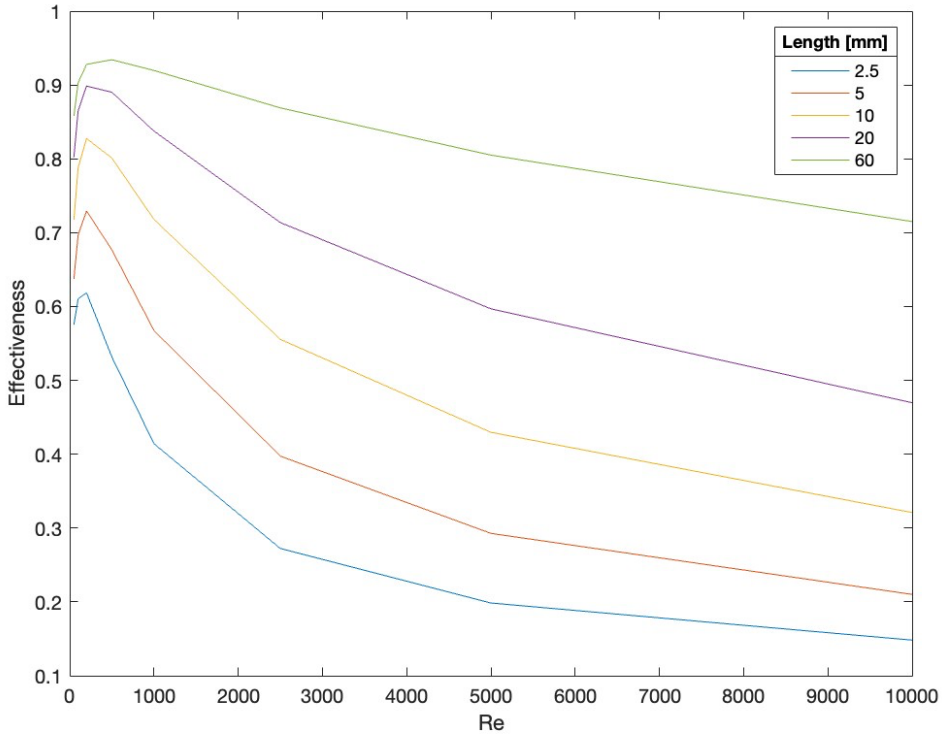

Figure 14 Nickel Counterflow One-Pass Heat Exchanger with 20 Square Channels at Size 0.05 mm and a Constant Wall and Membrane Thickness of 0.025 mm; Air as the Fluid with Hot Inlet at 815°C, Cold Inlet at 20°C, and 10 Bar Exit Pressure with Flows Balanced at a Reynold's Number Ranging From 50 to 10000; Insulated to Prevent Heat Loss to the Environment

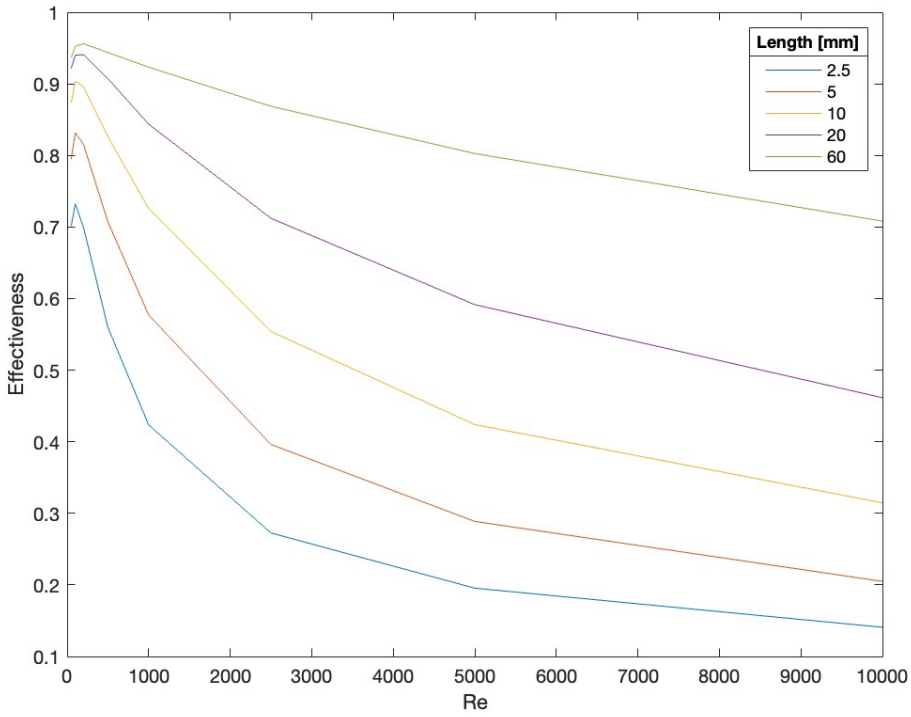

Figure 15 Alumina Counterflow One-Pass Heat Exchanger with 20 Square Channels at Size 0.05 mm and a Constant Wall and Membrane Thickness of 0.025 mm; Air as the Fluid with Hot Inlet at 815°C, Cold Inlet at 20°C, and 10 Bar Exit Pressure with Flows Balanced at a Reynold's Number Ranging From 50 to 10000; Insulated to Prevent Heat Loss to the Environment

Starting with nickel and alumina as the heat exchanger material, it is evident that lowering the thermal conductivity gets closer to the goal of a high peak effectiveness at low Reynold's numbers. For example, nickel surpasses the 0.9 effectiveness threshold, peaking at 0.934 at a Reynold's number of 500. However, even at the low Reynold's number range, the initially low effectiveness still persists, indicating axial conduction continues to limit performance.

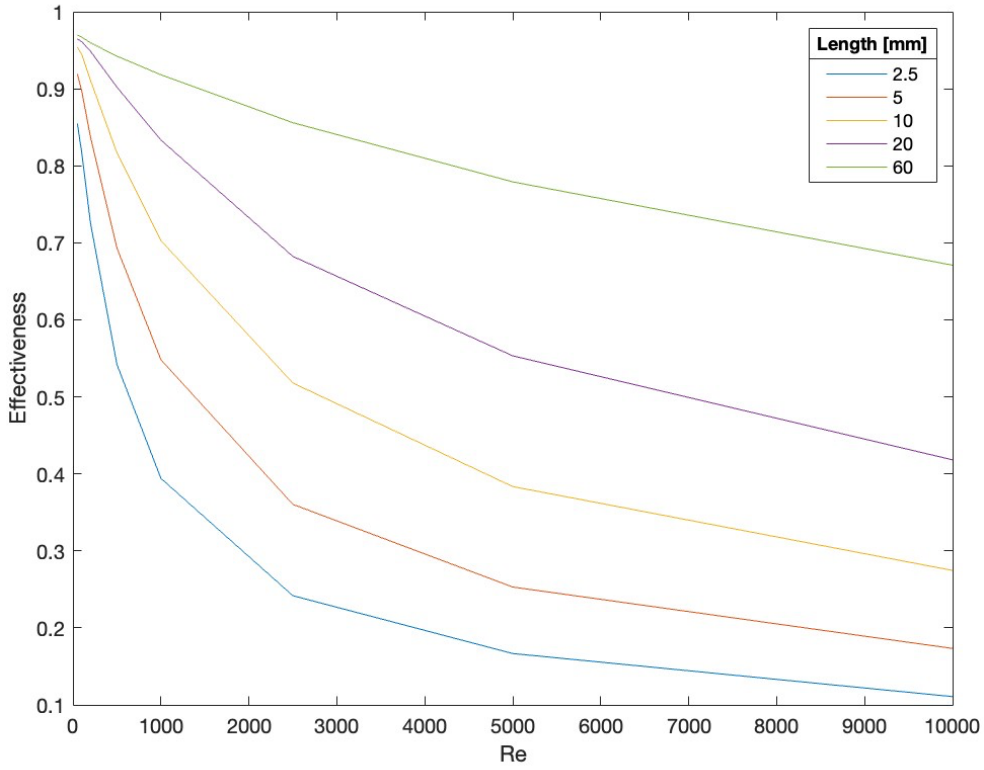

Figure 16 8YSZ Counterflow One-Pass Heat Exchanger with 20 Square Channels at Size 0.05 mm and a Constant Wall and Membrane Thickness of 0.025 mm; Air as the Fluid with Hot Inlet at 815℃, Cold Inlet at 20℃, and 10 Bar Exit Pressure with Flows Balanced at a Reynold's Number Ranging From 50 to 10000; Insulated to Prevent Heat Loss to the Environment

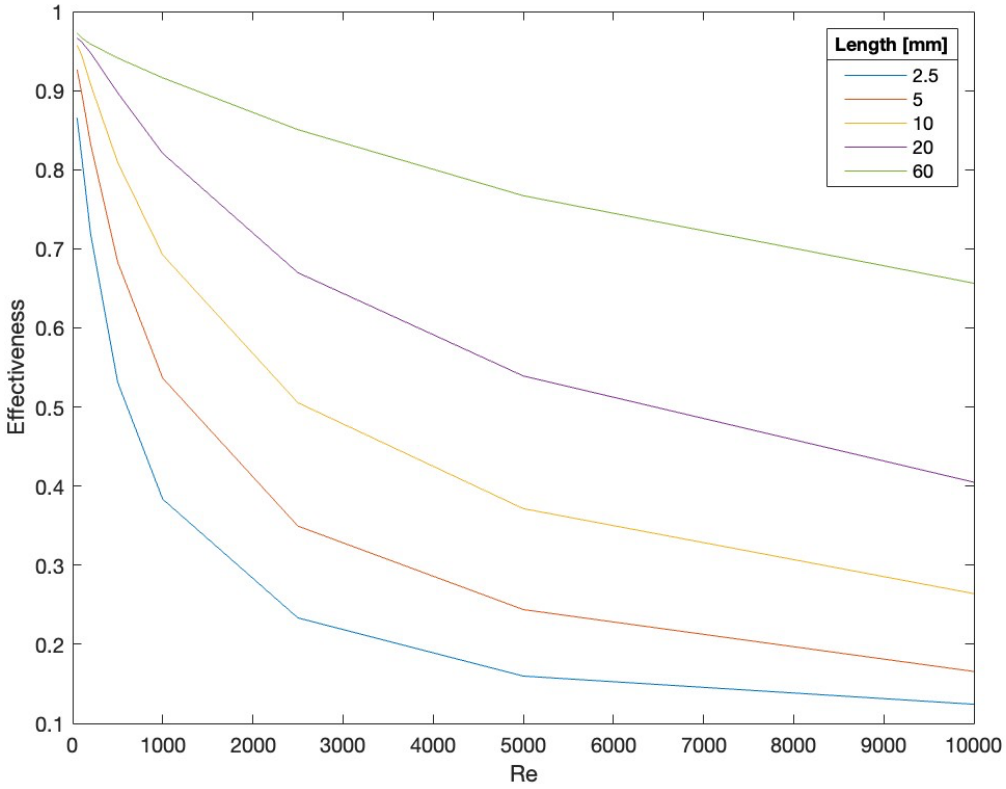

Figure 17 Glass Counterflow One-Pass Heat Exchanger with 20 Square Channels at Size 0.05 mm and a Constant Wall and Membrane Thickness of 0.025 mm; Air as the Fluid with Hot Inlet at 815℃, Cold Inlet at 20℃, and 10 Bar Exit Pressure with Flows Balanced at a Reynold's Number Ranging From 50 to 10000; Insulated to Prevent Heat Loss to the Environment

Comparing 8YSZ and glass to alumina shows an even better improvement in effectiveness with a higher peak at a lower flow rate, peaking at 0.596 at 200 Re. When the thermal conductivity is reduced to that of 8YSZ and glass, the effectiveness curves no longer have initially low effectiveness at low flow rates. Both reach their peak effectiveness at the lowest Reynold's number tested, reaching a maximum effectiveness of 0.970 for 8YSZ and 0.973 for glass. This suggests that axial conduction is sufficiently reduced at that thermal conductivity range to minimize the detrimental impact of axial conduction. Having peaks close

to one also indicates that the thermal conductivity is not too low to suppress heat transfer across the membrane.

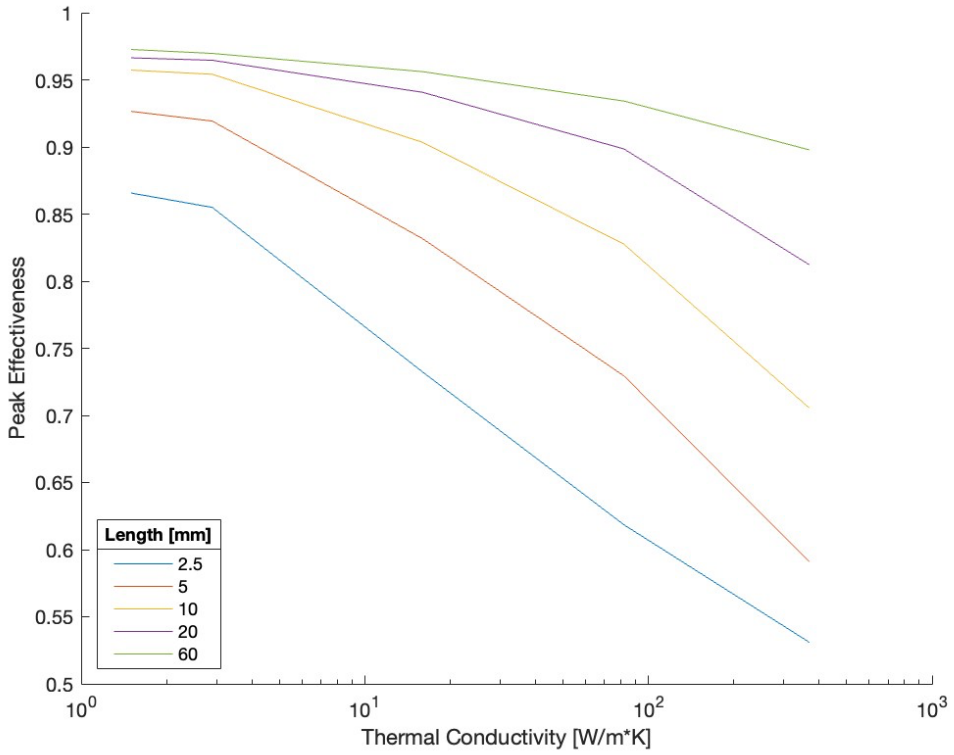

Figure 18 Counterflow One-Pass Heat Exchanger of Various Material Composition with 20 Square Channels at Size 0.05 mm and a Constant Wall and Membrane Thickness of 0.025 mm; Air as the Fluid with Hot Inlet at 815°C, Cold Inlet at 20°C, and 10 Bar Exit Pressure with Flows Balanced at a Reynold's Number Ranging From 50 to 10000; Insulated to Prevent Heat Loss to the Environment

Both thermal conductivity values lie in the ideal range of thermal conductivity for low flow rates, which can be seen in **Figure 18.** The figure highlights the peak effectiveness values for each thermal conductivity tested. The results indicate that effectiveness peaks in the single-digit range of thermal conductivity. However, increasing the length also yields considerable improvement in effectiveness, but with a diminishing return at longer lengths. Longer length heat exchangers also experience a wider range of acceptable thermal conductivity values near the

peak effectiveness. Still, maximum effectiveness is reached at all lengths using a thermal conductivity around 1 $\frac{W}{m \cdot K}$. The utilization of low thermal conductivity values enables equivalent effectiveness values as longer lengths at higher thermal conductivity, resulting in higher power density due to less material being required.

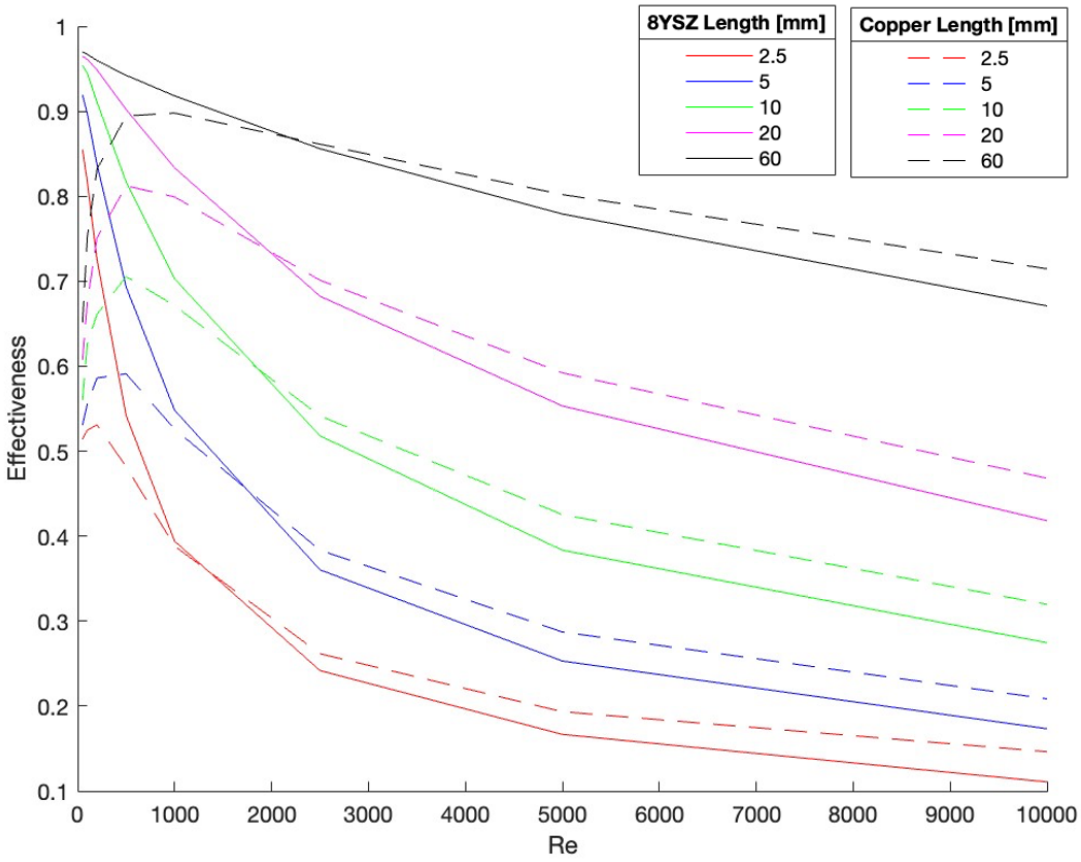

Figure 19 Comparison of 8YSZ and Copper Counterflow One-Pass Heat Exchangers of Various Material Composition with 20 Square Channels at Size 0.05 mm and a Constant Wall and Membrane Thickness of 0.025 mm; Air as the Fluid with Hot Inlet at 815°C, Cold Inlet at 20°C, and 10 Bar Exit Pressure with Flows Balanced at a Reynold's Number Ranging From 50 to 10000; Insulated to Prevent Heat Loss to the Environment

The caveat to those results is that the peak effectiveness values occur at different flow rates. **Figure 19** compares copper and 8YSZ to illustrate that the ideal thermal conductivity value will vary as flow rate changes. As shown, copper beings to outperform 8YSZ once Reynold's

number increases beyond the 1,000 to 2,000 range, depending on length. At short lengths, there is limited space for heat transfer to occur, reducing the time for heat transfer. Therefore, the intersection point occurs at a lower flow rate for the smallest heat exchanger because a high thermal conductivity is required to efficiently transfer heat over such short distances. On the other hand, the longest length shifts to a higher Reynold's value crossover point because of the increased time to transfer heat between the fluids. This phenomenon also explains the faster drop-off for YSZ effectiveness as Reynold's number continues to increase, since copper is able to transfer heat faster as flow rate limits the time the fluids have to exchange heat.

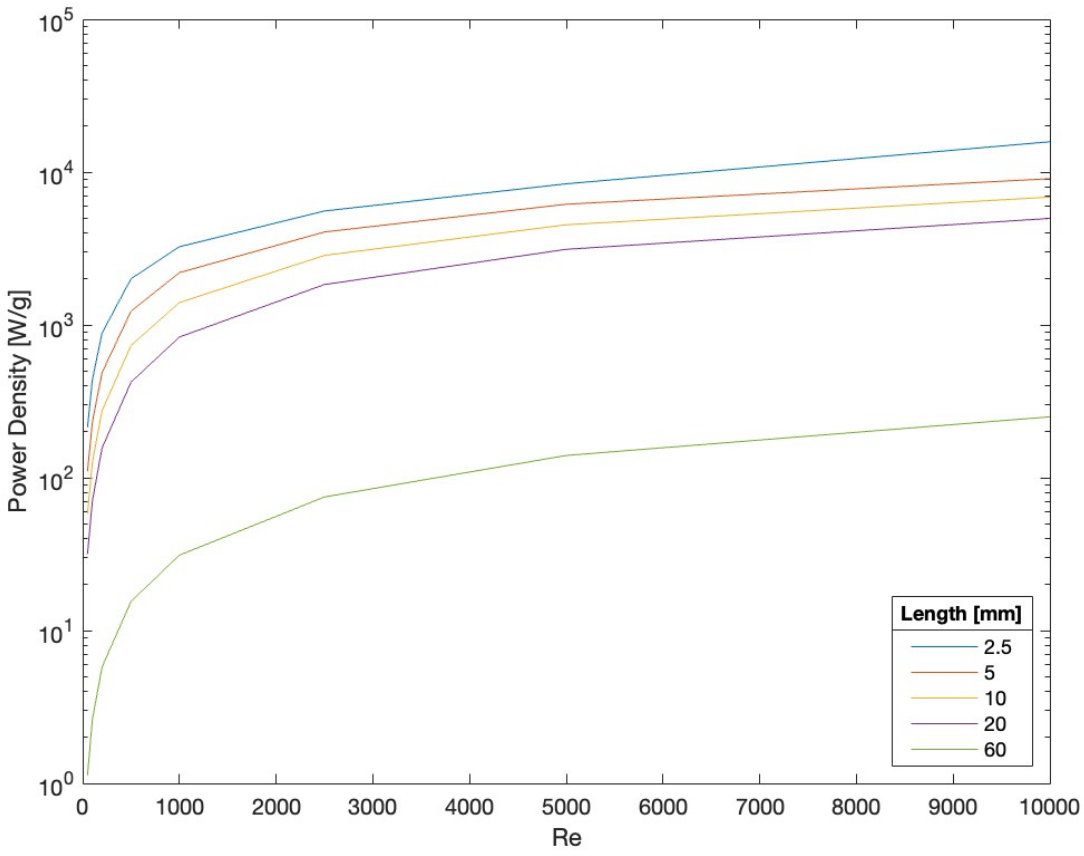

Figure 20 Copper Counterflow One-Pass Heat Exchanger with 20 Square Channels at Size 0.05 mm and a Constant Wall and Membrane Thickness of 0.025 mm; Air as the Fluid with Hot Inlet at 815°C, Cold Inlet at 20°C, and 10 Bar Exit Pressure with Flows Balanced at a Reynold's Number Ranging From 50 to 10000; Insulated to Prevent Heat Loss to the Environment

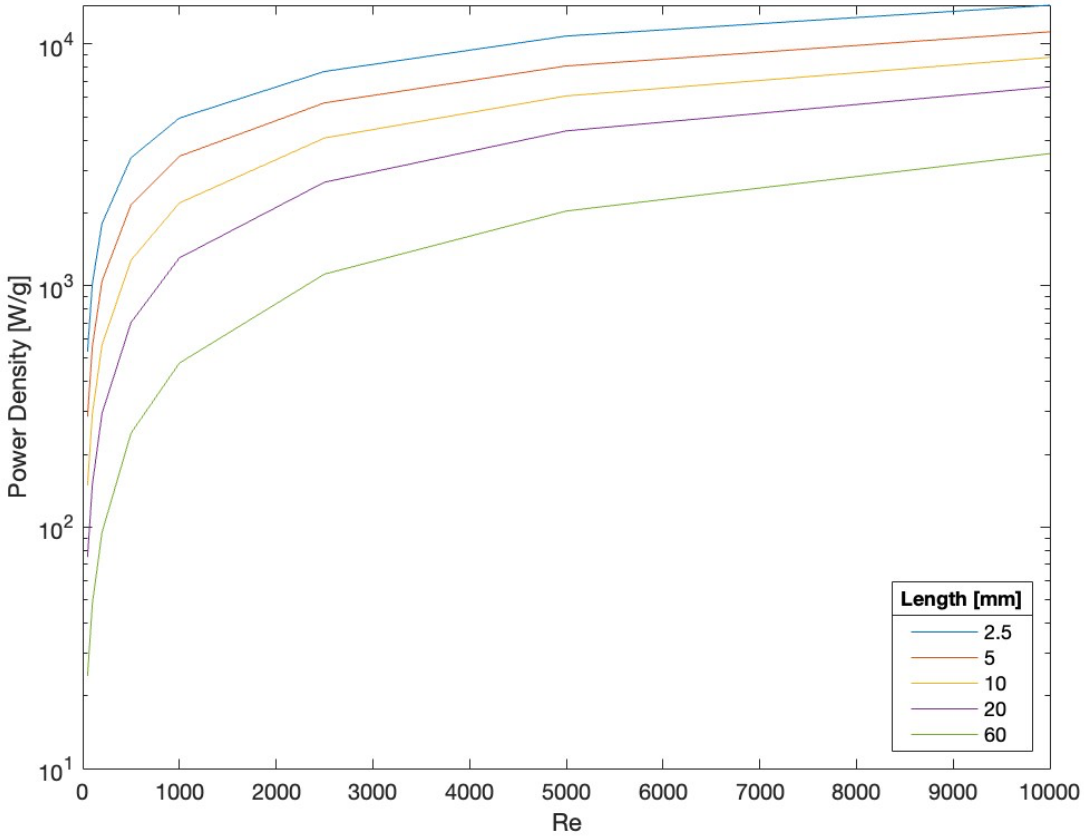

Figure 21 8YSZ Counterflow One-Pass Heat Exchanger with 20 Square Channels at Size 0.05 mm and a Constant Wall and Membrane Thickness of 0.025 mm; Air as the Fluid with Hot Inlet at 815℃, Cold Inlet at 20℃, and 10 Bar Exit Pressure with Flows Balanced at a Reynold's Number Ranging From 50 to 10000; Insulated to Prevent Heat Loss to the Environment

Figures 20 and **21** highlights the differences in power density between copper and 8YSZ. Apart from the 2.5 mm length model beyond a Reynold's number of 9000, 8YSZ always has a higher power density than copper due to increased effectiveness as axial conduction is reduce. As heat exchanger length increases, the difference in power density between the two expands. For example, at a Reynold's number of 1000, 8YSZ has a 1.52 times higher power density for 2.5 mm in length, compared to 15.3 times higher for 60 mm in length. This difference persists even

at low flow rates, showing that lowering the heat exchanger material's thermal conductivity to reduce axial conduction results in a higher power density.

After comparing changes to effectiveness and power density for different thermal conductivities, 8YSZ presents itself as a suitable candidate for high performance microchannel heat exchanger applications. It has a thermal conductivity within the ideal range to reach an effectiveness close to one at low flow rates required by pressure drop by limiting axial conduction, while still allowing enough heat to transfer between the fluid streams.

In addition, 8YSZ possesses beneficial qualities that make it promising candidate for high performance microchannel heat exchangers used in SOC applications. Its high mechanical stress and fracture toughness allows it to withstand the pressure gradient associated with microchannels, while its thermal shock resistance permits it to operate in the extreme temperature gradient needed for SOFC and SOEC conditions. Additionally, its robust chemical stability allows it to function in the presence of the various gases without degradation. Lastly, 8YSZ is commonly used as the electrolyte material for fuel and electrolysis cells, so the heat exchanger will have a matching thermal expansion coefficient, allowing it to be co-sintered with the fuel or electrolysis stack [39,40]. Typical drawbacks of using 8YSZ include challenges to manufacture, especially at micron the scale, which increases complexity and cost to manufacture. However, dry-powder additive manufacturing has demonstrated the ability to manufacture ceramic microchannels at this scale, overcoming these previous obstacles.

CHAPTER FIVE: MULTI-PASS SYSTEM

Analysis into a heat exchanger's channel dimensions, flow rate, and thermal conductivity of the heat exchanger material suggests that a multi-pass system could possibly outperform one-pass designs to achieve both an effectiveness close to one as well as a higher power density than a one-pass system. Pressure drop is the limiting factor that lowers performance and optimization of a one-pass system. Small channel dimensions are desirable because of their high power density, but the pressure drop is significant with even moderate flow rates. To keep the pressure difference at an acceptable level, the flow rate needs to be kept considerable low or the length of the system needs to be kept short. Both options lower the maximum possible effectiveness of the system, necessitating a design change to reach both high power density and high effectiveness.

The multi-pass system is designed to keep the pressure drop at an acceptable level, with additional measures to raise the effectiveness of the system. It deals with the issue of pressure drop by stacking the one-pass designs on top of one another. Doing so allows for each layer to be short in length, allowing the flow rate to increase and still result in low pressure drop for each layer. The exhaust from each layer is then transferred to the next layer by gas routing in the external manifold that surround the system. Even with the increased mass associated with this design coming from stacked layers, it can still achieve higher power density than the one-pass systems because it would not be limited by an effectiveness limit.

Despite the advantages, several potential downsides may arise. First, manufacturing becomes more complex compared to creating a one pass system, especially with ceramic material that is compatible with SOCs. However, the manufacturing process can be more simplistic than creating long channels with thin walls and membrane due to machining size limitations. The dry-powder additive manufacturing method shown in the CESI lab allows for the creation of stacked microchannel layers, negating this issue. Another drawback is the potential introduction of additional structural challenges that come from stacking repeated layers on top of one another. These issues include the additional weight on the membrane and walls, thermal stresses, and compounding pressure gradients between stacked layers. Balancing the flows inside the channels becomes a challenge as external gas routing may lead to unevenly distributed flow, potentially causing over pressurization and structural failure.

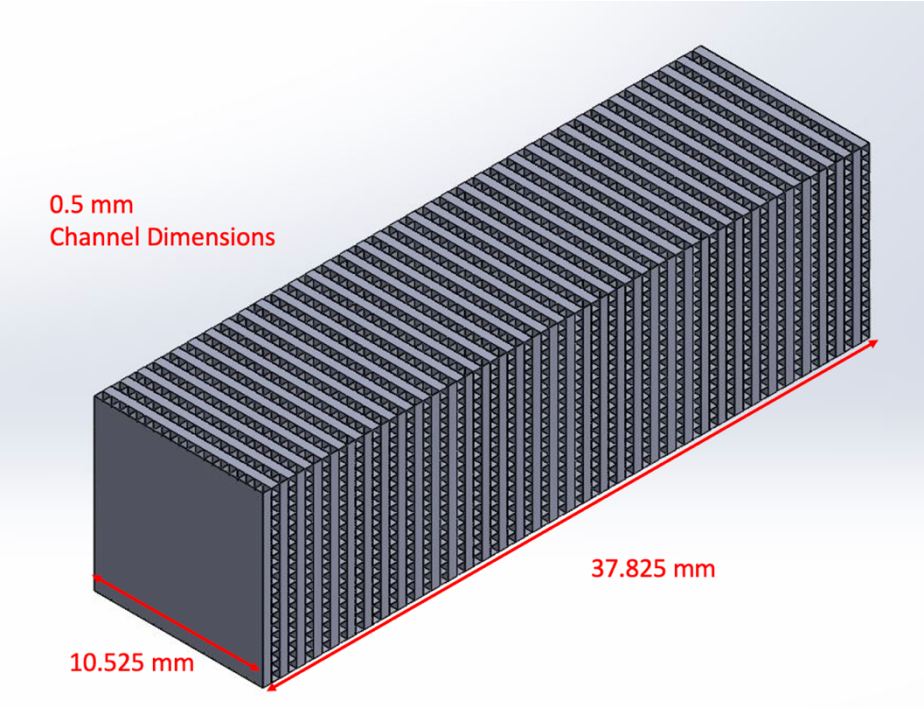

Figure 22 Multi-pass Heat Exchanger at 0.05 mm Square Channel Size with 20 Channels Per Layer, Two Layers per Pass, and 36 Total One-Pass Layers

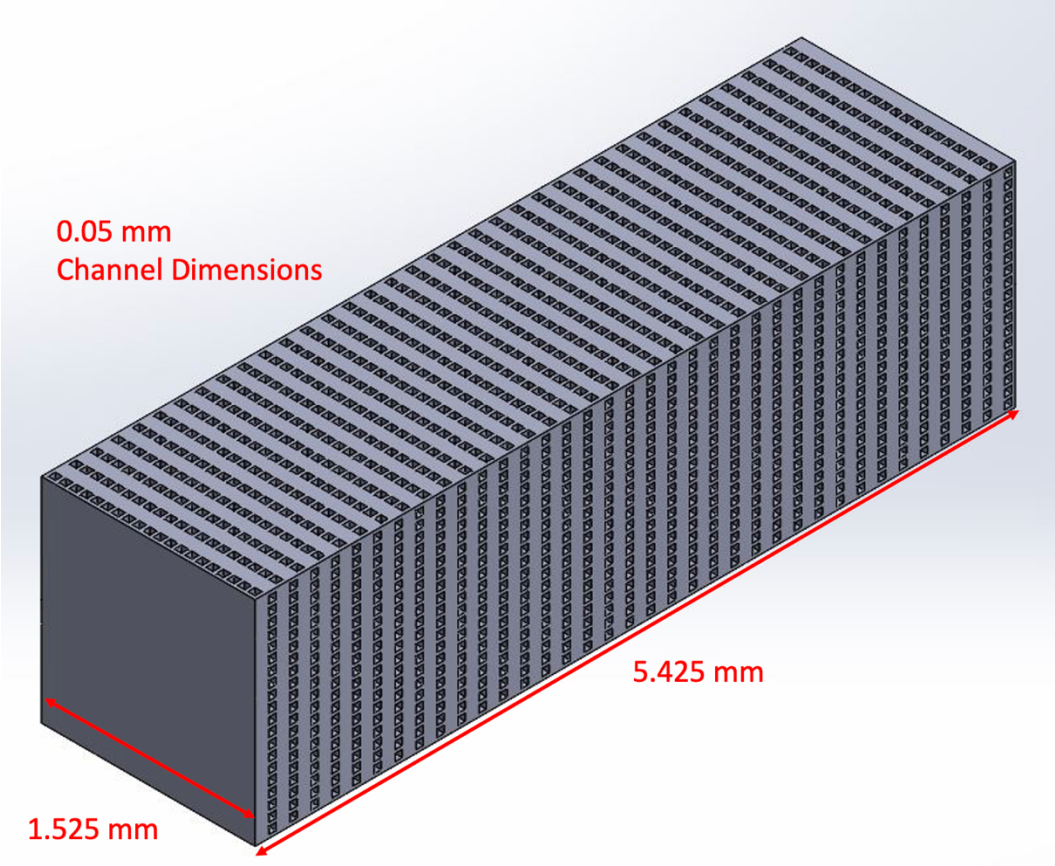

Figure 23 Multi-pass Heat Exchanger at 0.05 mm Square Channel Size with 20 Channels Per Layer, Two Layers per Pass, and 36 Total One-Pass Layers

Figures 22 and **23** show the CFD models used to test the performance of a multi-pass, counterflow heat exchanger. The first heat exchanger, shown in **Figure 22**, has square channel dimensions of 0.05 mm, while the second model, in **Figure 23**, has larger channel dimensions at 0.5 mm. To accurately compare the results of these models to the one-pass systems, the geometry of the heat exchanger matches that of the previous models. Both have a counterflow design, with each fluid starting at opposite ends of the heat exchanger. Creating such geometries gives the 0.5 mm design a length of 10.525 mm, while the 0.05 mm design has a length of 1.525 mm. 8YSZ

comprises the heat exchanger material as it limits axial conduction and still allow for an effectiveness close to one. Finally, each system contains 36 one-pass layers per fluid.

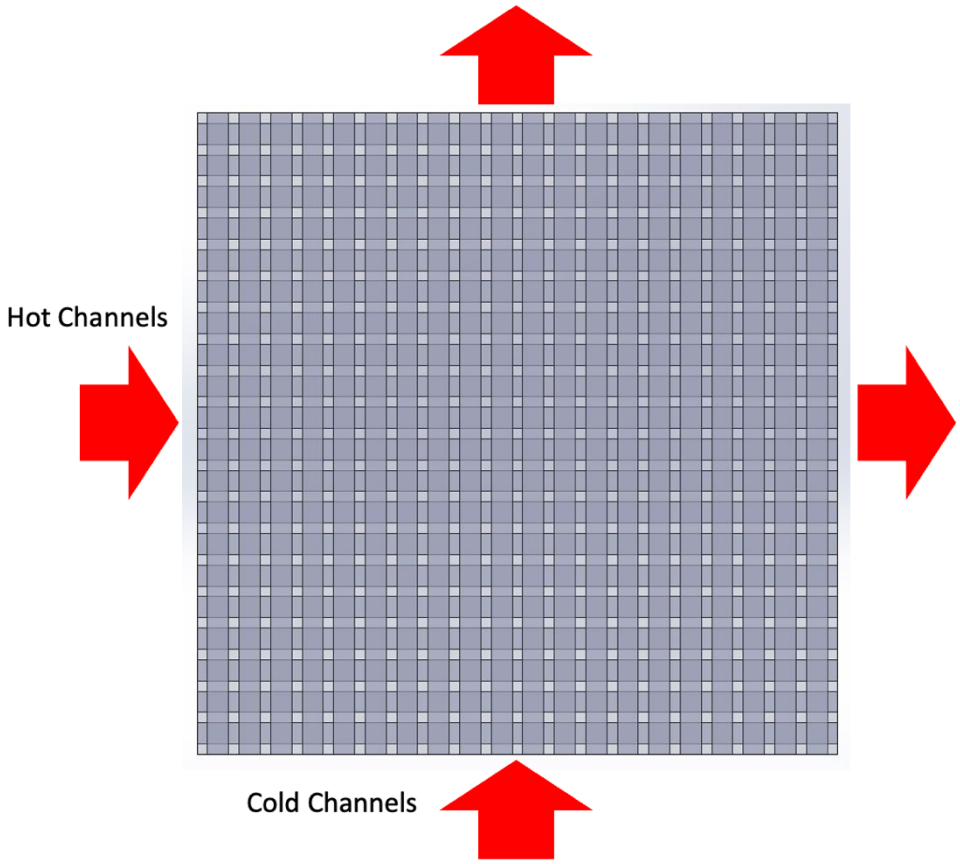

Figure 24 Multi-pass System Crossflow Pattern Between Hot and Cold Layers

The heat exchangers are counterflow in the fact that both fluids start on opposite ends of the heat exchanger to achieve high effectiveness. However, each layer is designed in crossflow routing orientation, which varies from previous one-pass designs. The crossflow pattern is used to prevent structural issues that come with channels stacked parallel on each other. **Figures 24-26** show the counterflow aspect as well as the crossflow pattern of heat transfer between the hot and cold layers.

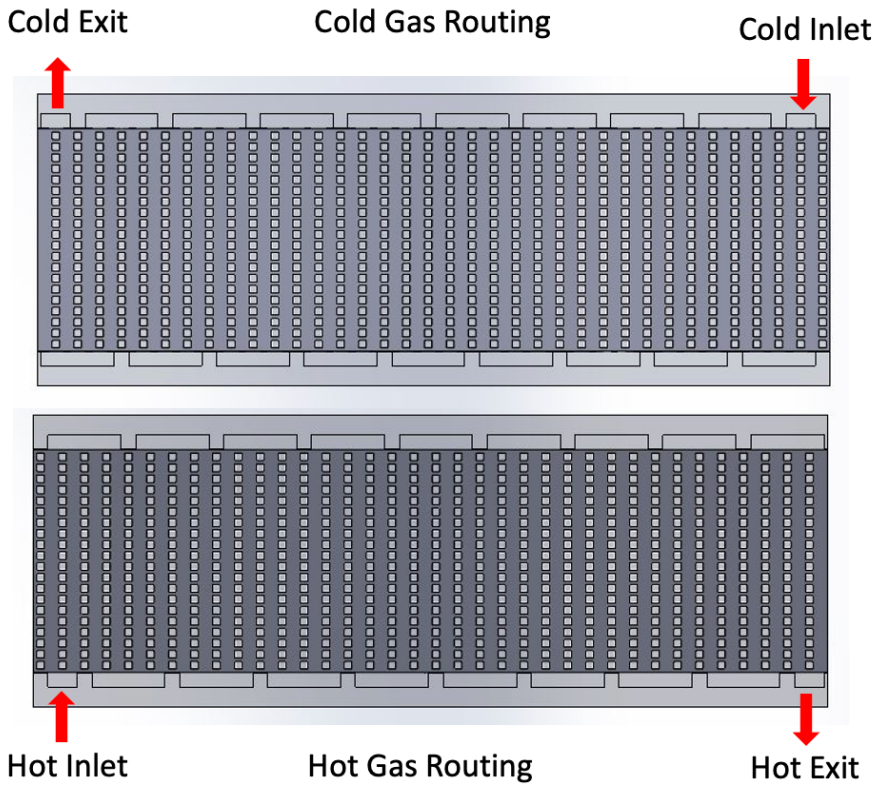

Figure 25 Multi-Pass Heat Exchanger Counterflow Pattern Through the External Manifold. Cold and Hot Gas Layers Oriented 90° From Each Other

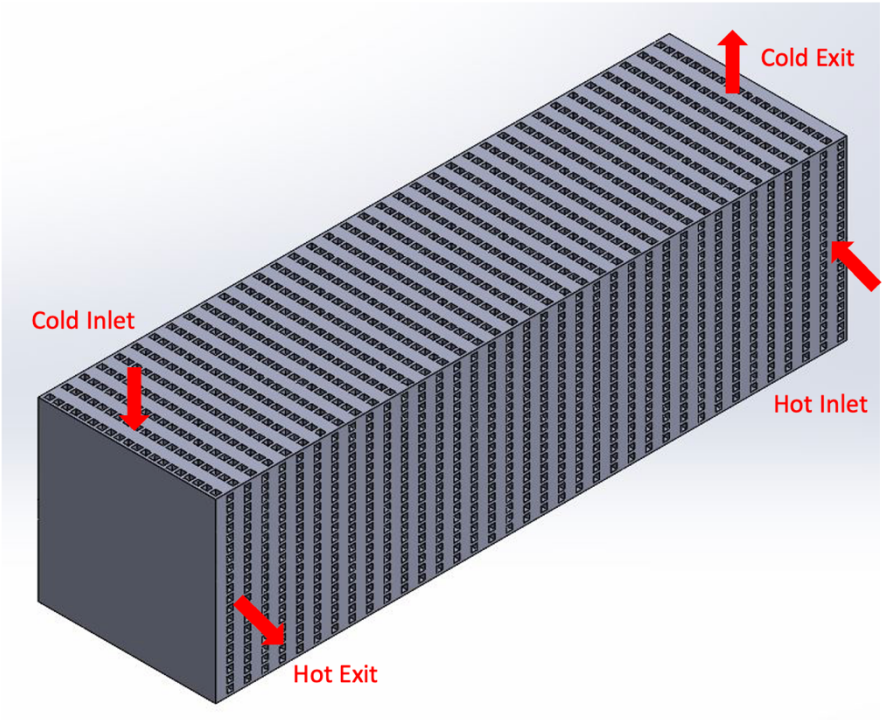

Figure 26 Multi-Pass System Gas Inlets and Exits

Another notable difference is the initial solid temperature of the heat exchanger material. For a one-pass system like the models used previously, each fluid channel is surrounded by insulation on all sides except the membrane. However, for a multi-pass system, each fluid channel is surrounded by heat exchanger material from another layer. This allows for greater heat dissipation from the hot fluid into the surrounding material. For one-pass systems, all the heat is transferred through the membrane, so it could reach an effectiveness close to one with the material having an initial solid temperature of 20℃. For the multipass design to reach a high effectiveness, the system needs to be preheated. For the CFD simulations, the initial solid temperature is set to 815 ℃.

Figure 27 Gas Routing Highlighting Two Layers per Pass using an External Manifold; 0.05 mm Channel Dimensions with Vertical Multi-Pass System

The last major difference also comes from the insulation, since the surrounding insulation routes the gases from one layer to the next. **Figure 27** shows the insulation manifold that routes the gases between layers and insulates it from the environment to prevent heat loss. It depicts the gas routing pattern and how two layers of fluid are transferred per pass. Each fluid is separately contained by the manifold, preventing the two from mixing. The cold fluid is routed through the top and bottom of the system, while the cold fluid travels through only the right and left sides. Insulation caps are placed on the front and back of the system to prevent heat from being lost to the environment, which can be seen in **Figure 28**.

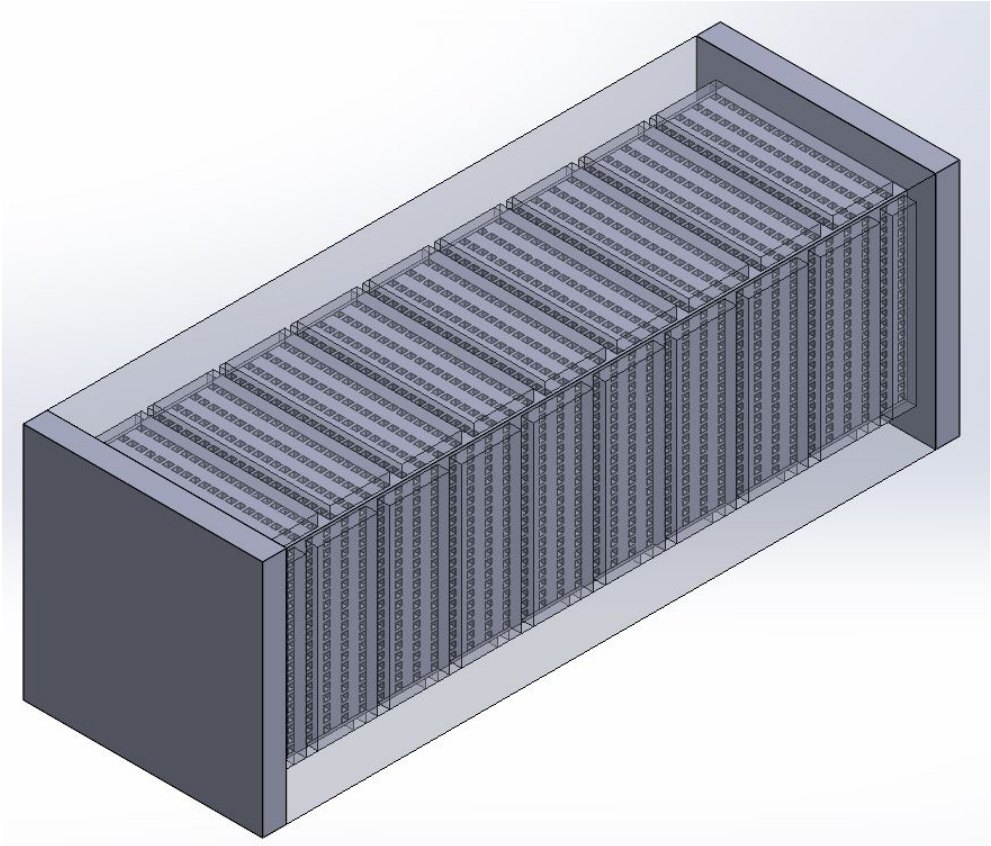

Figure 28 Multi-Pass System with Insulated Caps at each End to Prevent Heat Loss along with Transparent Insulated Manifold

The purpose behind this set of models is to determine if a multi-pass system outperforms one-pass systems by reaching a higher effectiveness and power density, indicating that design optimization is required for high performance microchannel heat exchangers. The two multi-pass systems have different channel dimensions, enabling a comparison of how varying channel dimensions differs in performance. Using the same channel dimensions as the previous models also allows for the comparison of multi-pass systems to one-pass systems.

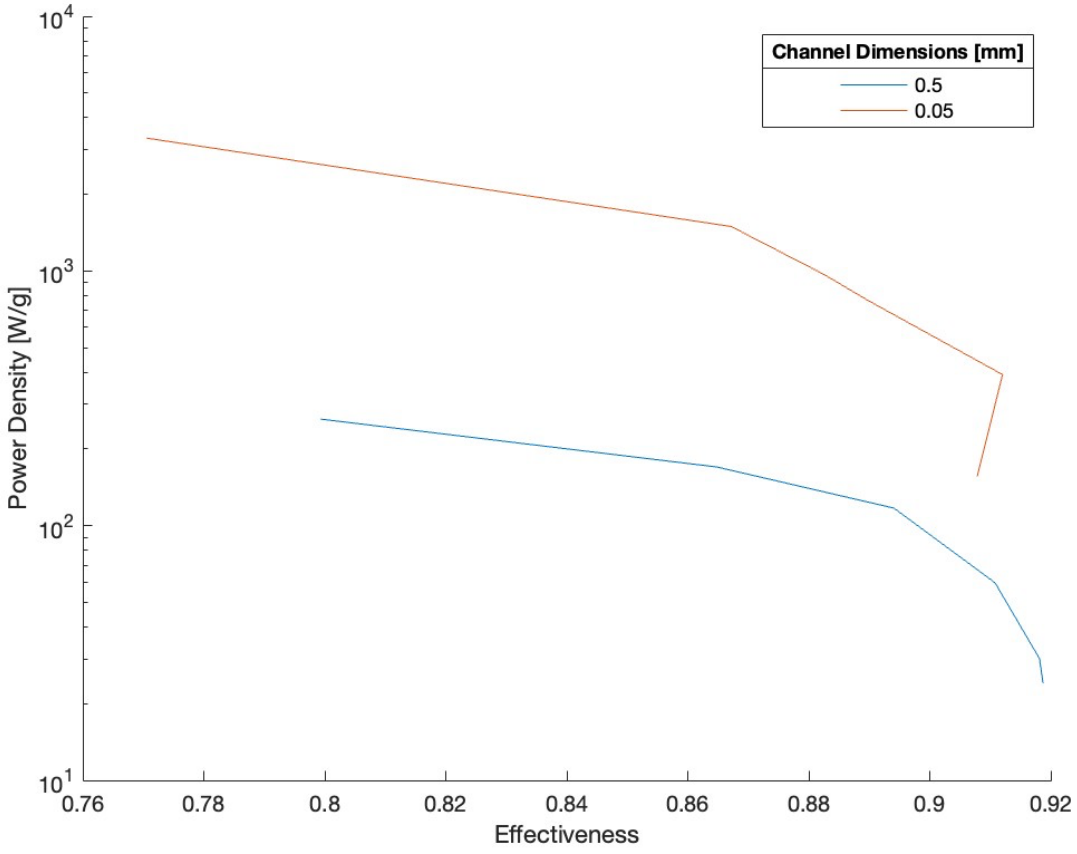

Figure 29 Multi-pass Counterflow 8YSZ Heat Exchanger at 0.05 mm and 0.5 mm Square Channel Sizes with 20 Channels Per Layer, Two Layers per Pass, and 36 Total One-Pass Layers at a Constant Wall and Membrane Thickness of 0.025 mm; Air is the Working Fluid with Hot Inlet Set at 815 and Cold Inlet at 20°C while the Initial Solid Temperature is at 815°C; Exit Pressurized to 10 Bar; Balanced Flow Rates Ranging from Reynold's Number of 200 to 5,000; Insulated to Prevent Heat Loss

Figure 29 depicts the result of changing channel dimensions for a multi-pass heat exchanger across various flowrates. Similar to the results of one pass systems, shrinking channel dimensions yields a lower maximum effectiveness and an order of magnitude increase in power density coming from the volume differences. Both heat exchangers experience a maximum effectiveness above 0.91, with the 0.05 mm channels only 0.0069 less than the 0.5 mm channel system. The smaller sized system reaches a maximum power density around 3300 W/g. At its peak effectiveness, it has power density of 390 W/g, which is a considerable improvement over the power density of 24 W/g the 0.5 mm system reaches at its maximum effectiveness.

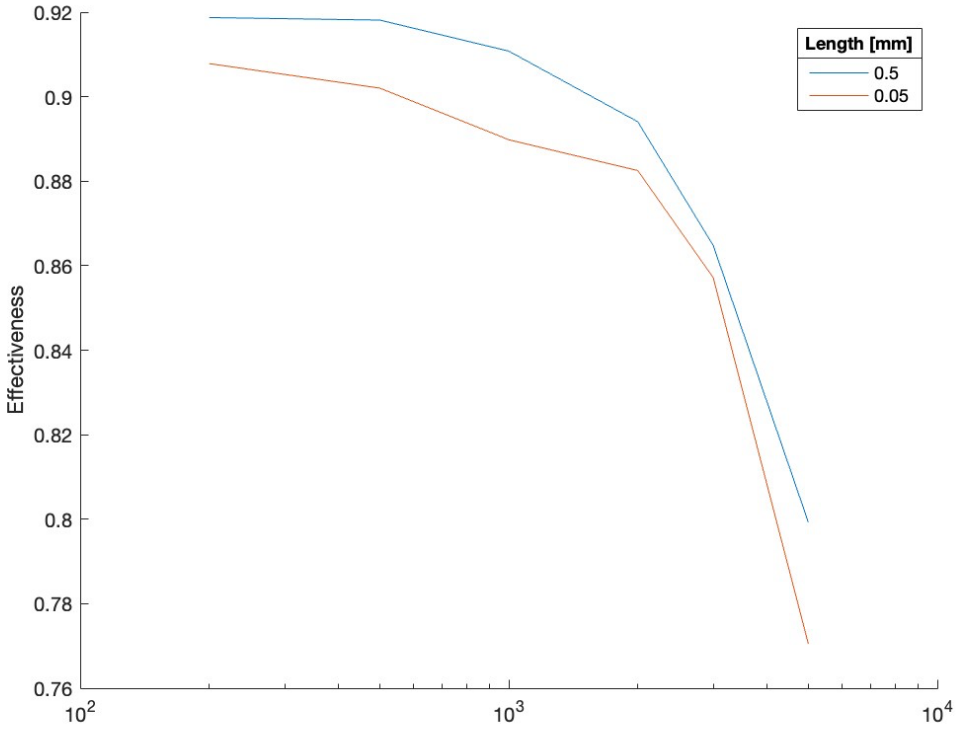

Figure 30 Effectiveness as a Function of Reynold's Number for a Multi-pass Counterflow 8YSZ Heat Exchanger at 0.05 mm and 0.5 mm Square Channel Size with 20 Channels Per Layer, Two Layers per Pass, and 36 Total One-Pass Layers at a Constant Wall and Membrane Thickenss of 0.025 mm; Air is the Working Fluid with Hot Inlet Set at 815 and Cold Inlet at 20°C while the Initial Solid Temperature is at 815°C; Exit Pressurized to 10 Bar; Balanced Flow Rates Ranging from Reynold's Number of 200 to 5,000; Insulated to Prevent Heat Loss

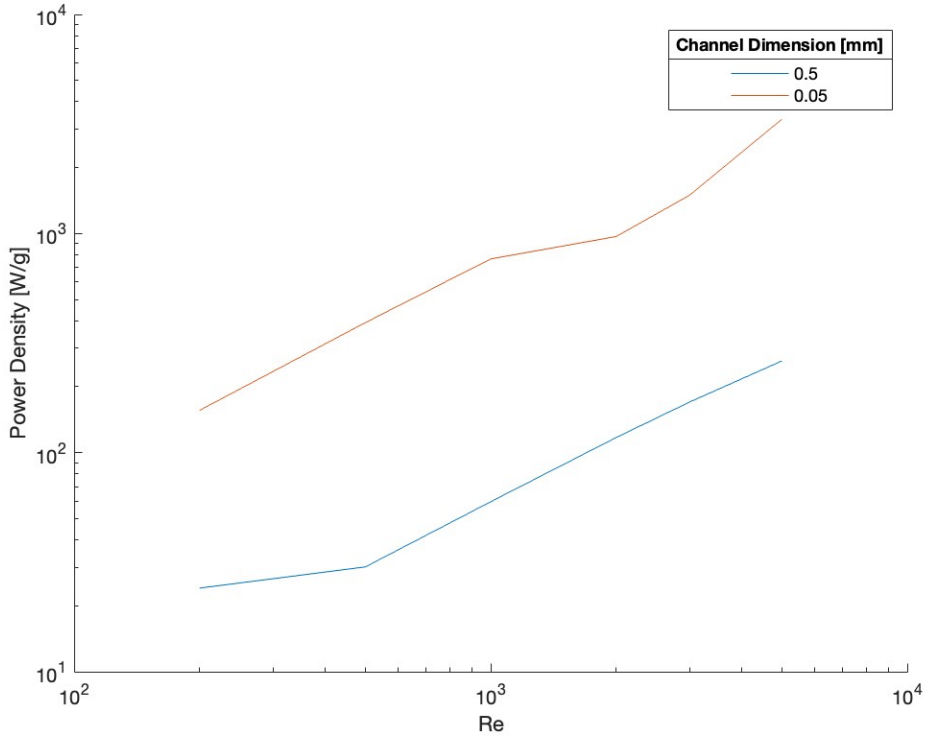

Figure 31 Power Density as a Function of Reynold's Number for a Multi-pass Counterflow 8YSZ Heat Exchanger at 0.05 mm and 0.5 mm Square Channel Size with 20 Channels Per Layer, Two Layers per Pass, and 36 Total One-Pass Layers at a Constant Wall and Membrane Thickenss of 0.025 mm; Air is the Working Fluid with Hot Inlet Set at 815 and Cold Inlet at 20℃ while the Initial Solid Temperature is at 815℃; Exit Pressurized to 10 Bar; Balanced Flow Rates Ranging from Reynold's Number of 200 to 5,000; Insulated to Prevent Heat Loss

Another takeaway from the simulation results is the considerable difference in performance across a range of flowrates. To further study this behavior, **Figures 30** and **31** displays how flow rate impacts both effectiveness and power density. The first plot illustrates how effectiveness falls off at high Reynold's values, with both systems experiencing similar performance patterns. Interestingly, both systems maintain an effectiveness over 0.90 below a

Reynold's number of 1000. In terms of power density, both systems also show similar behavior as both experience a power-law relationship. Combining the results from both plots indicates that multi-pass systems can increase flow rate to a higher range to get increased power density while still maintaining a relatively high effectiveness, despite the tradeoff between the two.

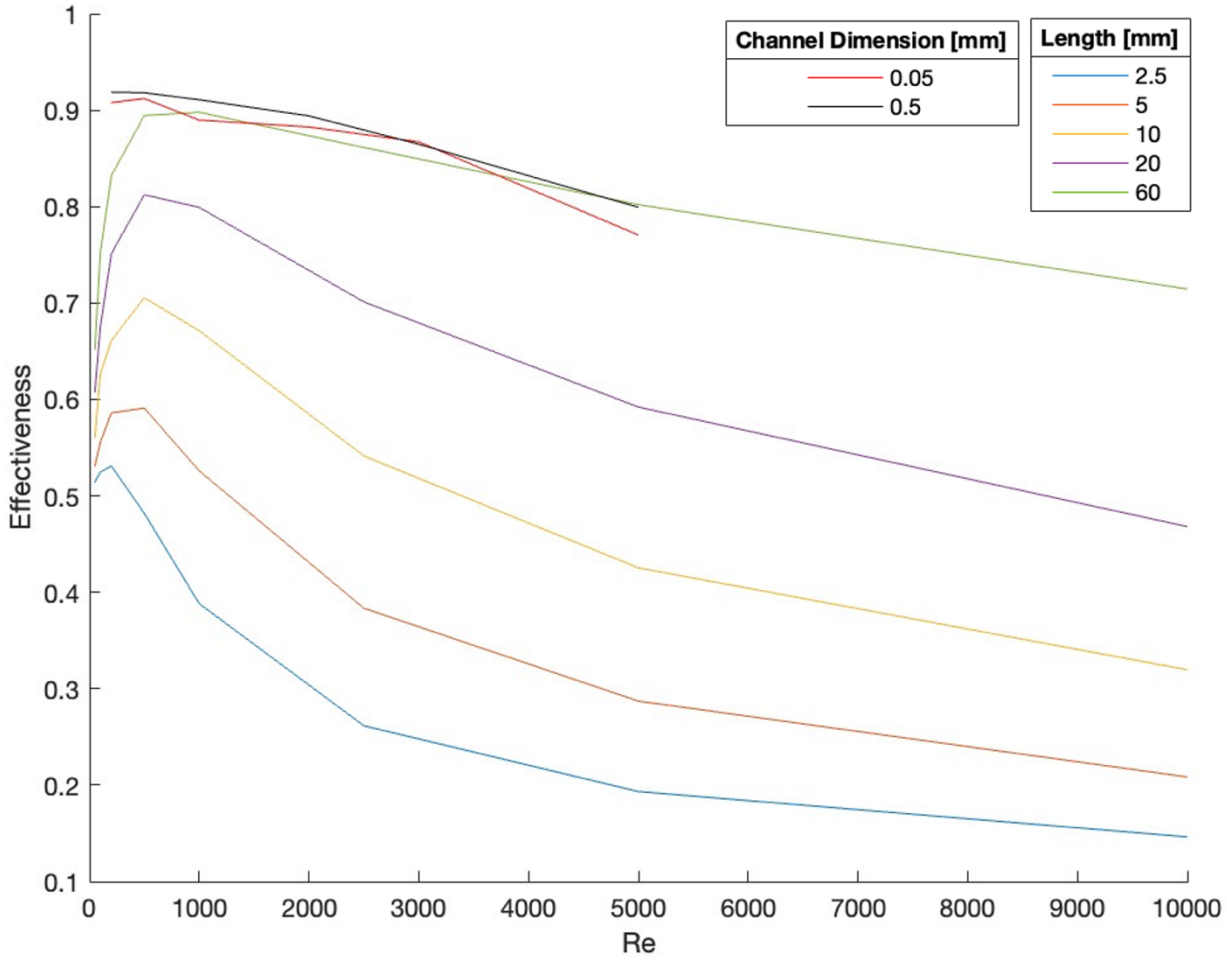

Figure 32 Comparison of 8YSZ Multi-Pass Systems and One-Pass Copper Systems; Copper Counterflow One-Pass Heat Exchanger with 20 Square Channels at Size 0.05 mm with Reynold's Number Ranging from 50 to 10000 and an Initial Solid Temperature of 20°C; 8YSZ Multi-Pass Counterflow Heat Exchanger at 0.05 mm and 0.5 mm Square Channel Sizes with 20 Channels Per Layer, Two Layers per Pass, and 36 Total One-Pass Layers with Reynold's Number Ranging from 200 to 5000 and an Initial Solid Temperature of 815°C; Both Systems Contain a Constant Wall and Membrane Thickenss of 0.025 mm; Air as the Working Fluid with Hot Inlet Set at 815°C and Cold Inlet at 20°C; Exit Pressurized to 10 Bar; Balanced Flow Rates; Insulated to Prevent Heat Loss

Shown in **Figure 32**, the performance of both multi-pass systems is compared to a copper one-pass heat exchanger with 0.05 mm square channels across various flowrates. Most notable is the high effectiveness at low Reynold's number regimes, where pressure drop is minimized through restricting the flow rates. Due to its ceramic composition, the tower design does not experience a decreased effectiveness coming from axial conduction that the copper heat exchangers experiences at low flow rates. The multi-pass systems then closely follow the performance curve of the 60 mm one-pass system as the flow rate increases. Considering the manufacturing constraints limiting the overall possible length of the one-pass system, the multi-pass system outperforms one-pass copper designs at more realistic lengths. Finally, both multi-pass systems have closely matched performances, with minimal increase in effectiveness for the 0.5 mm design.

Since axial conduction drives down the effectiveness of one-pass systems at low flow rates, the performance of the multi-pass systems is compared to an 8YSZ one-pass heat exchanger with 0.05 mm square channel dimensions, show in **Figure 33**.

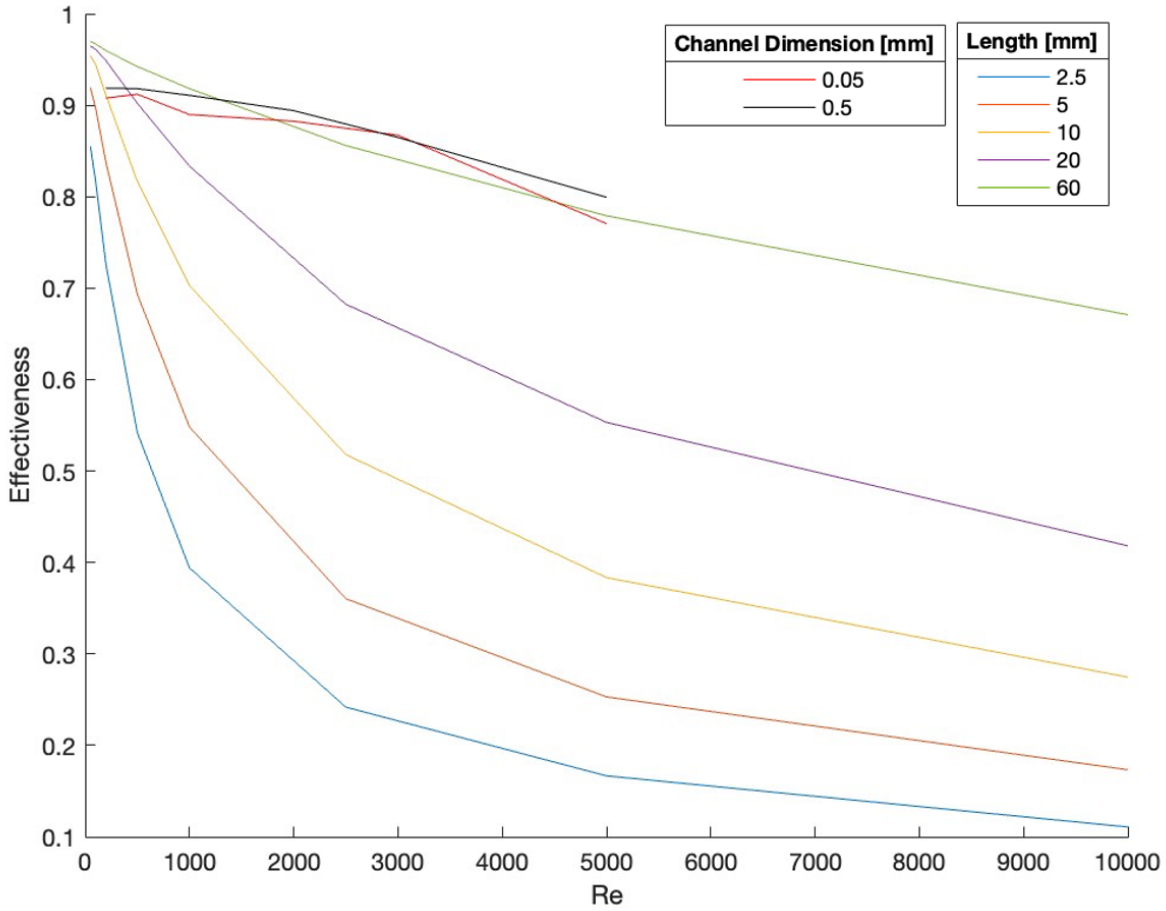

Figure 33 Comparison of 8YSZ Multi-Pass Systems and One-Pass 8YSZ Systems; 8YSZ Counterflow One-Pass Heat Exchanger with 20 Square Channels at Size 0.05 mm with Reynold's Number Ranging from 50 to 10000 and an Initial Solid Temperature of 20°C; 8YSZ Multi-Pass Counterflow Heat Exchanger at 0.05 mm and 0.5 mm Square Channel Sizes with 20 Channels Per Layer, Two Layers per Pass, and 36 Total One-Pass Layers with Reynold's Number Ranging from 200 to 5000 and an Initial Solid Temperature of 815°C; Both Systems Contain a Constant Wall and Membrane Thickenss of 0.025 mm; Air as the Working Fluid with Hot Inlet Set at 815°C and Cold Inlet at 20°C; Exit Pressurized to 10 Bar; Balanced Flow Rates; Insulated to Prevent Heat Loss

Since axial conduction no longer drives suppresses the effectiveness at low Reynold's values, the one-pass heat exchangers reach a higher effectiveness at the lowest flow rates tested beyond 5 mm in length. However, as Reynold's number begins to increase, the one-pass systems experience a significant decline in effectiveness compared to the multi-pass system. The multi-

pass systems reach a higher effectiveness than all one-pass heat exchangers, regardless of length, beyond a Reynold's number of 2000 up to 5000.

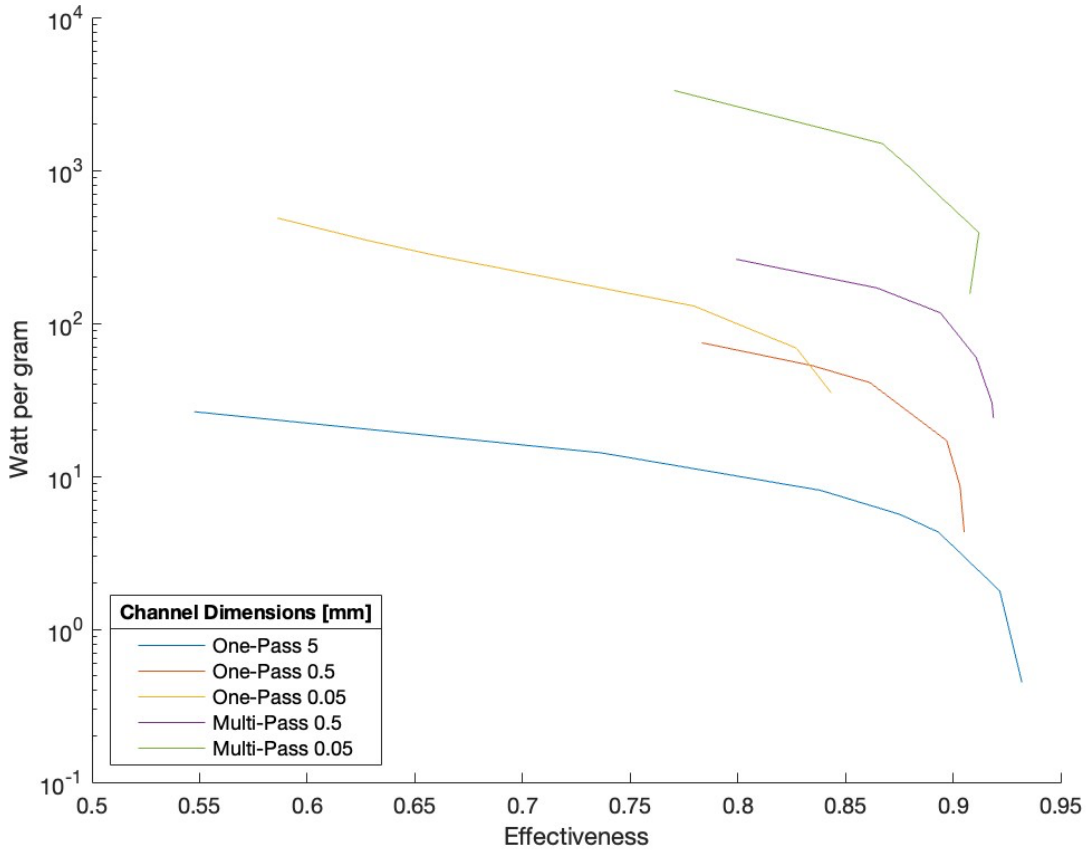

Figure 34 Comparison of One-Pass Heat Exchanger Performance at 200 Re with Varying Channel Dimensions and Lengths to Multi-Pass Systems with Varying Reynold's Number

To highlight the differences in power density of the multi-pass system compared to the one pass systems, **Figure 34** compares copper one-pass heat exchangers at a constant Reynold's number of 200 with varying lengths and channel dimensions to both 8YSZ multi-pass systems with flow rates ranging from a Reynold's number of 200 to 5000. Both multi-pass systems reach a higher power density than their one-pass counterparts at the same channel dimensions. Even

the 0.5 mm channel size multi-pass system reaches a higher power density than the one-pass systems with a smaller channel size of 0.05 mm.

CHAPTER SIX: CONCLUSION

CFD simulations were conducted on a counterflow one-pass square, microchannel heat exchanger, consisting of 20 channels with a constant membrane and wall thickness of 25 μm. Flow rates are balanced as hot air entered the heat exchanger at 815℃ while cold air entered at 20℃. The outlet boundary condition is set to 10 bar environmental pressure. Only the walls and membrane consisted of the heat exchanger material, as the channels were insulated to prevent heat loss to the environment.

The first set of simulations varied channel and length dimensions between 5, 0.5, and 0.05 mm for a copper heat exchanger. The length scales tested for the 5 mm channels were 0.5, 1.0, 2.5, 5.0, and 10 meters, with 0.5 mm and 0.05 mm decreasing in length by a factor of 10 and 100, respectively. Two flow rates were tested, corresponding to a Reynold's number in the channel of 200 and 1000. Using these simulations, it is found that:

1) Decreasing the channel dimensions from 5 mm to 0.5 mm resulted in a 9.6 times increase in power density and a 8.7 times increase in power density going from 0.5 mm to 0.05 mm demonstrating the increase in power density that comes with shrinking channel dimensions.
2) Longer channels require longer lengths to reach similar effectiveness values, resulting a tradeoff between increased effectiveness and decreased power density due to the increased mass of a longer heat exchanger.

3) Reducing channel dimensions at constant length result in both an increase in effectiveness and power density at a Reynold's number of 1000. However, this advantage diminishes as length is increased.
4) Each channel dimension varied in its peak effectiveness value, with smaller channels experiencing a lower peak effectiveness.
5) As the effectiveness nears its peak, there is an exponential decay in power density as increasing the length of the heat exchanger does not bring significant additional heat transfer to increase effectiveness and only increases the total mass.
6) Miniaturization improves heat exchanger performance across multiple dimensions while constraining the maximum effectiveness and raising the pressure drop.
7) At a Reynold's number of 200, reducing channel dimensions led to a lesser increase in power density when compared to a Reynold's number of 1000.
8) At sufficient lengths, larger channels can become objectively better as they reach higher power density and effectiveness.
9) The 0.05 mm channel dimension experienced a more uniform cross-sectional temperature distribution compared to 0.5 mm and 5 mm channels, despite a lower fluid velocity. This comes from axial conduction being more pronounced due to higher heat transfer rates with the walls and membrane.
10) The 0.05 mm channel dimension also experienced the most uniform temperature distribution as heat is transferred from the membrane, indicating high effectiveness performance is possible at low flow rates if axial conduction can be reduced.

The second set of simulations varied Reynold's number in the channel for a copper heat exchanger with 0.05 mm channels at 2.5, 5, 10, 20, and 60 mm in length. It was shown that:

11) At all length, a copper heat exchanger is limited in its maximum possible effectiveness due to axial conduction. Flow rates must be increased to overcome axial conduction, with longer lengths requiring high flow rates.

The third set of simulations ran the same Reynold's number sensitivity test for heat exchangers with 0.05 mm channels, but changed the heat exchanger material to nickel, alumina, 8YSZ, and glass to test the effects of reducing thermal conductivity. Doing so proved:

12) As thermal conductivity was reduced, the peak effectiveness increased and occurred at lower Reynold's numbers.
13) Glass and 8YSZ had no initial effectiveness drop by limiting axial conduction. Both reached peak effectiveness values greater than 0.95 at the lowest flow rate tested.
14) The ideal thermal conductivity range that led to the highest effectiveness occurred at a thermal conductivity of $1\ \frac{\mathrm{W}}{\mathrm{m \cdot K}}$. At longer lengths, the peak thermal conductivity range increased to higher values.
15) Copper begins outperformed 8YSZ in effectiveness between 1000 and 2000 Re depending on the length scale, with 8YSZ outperforming copper at lower Reynold's values.

Based on the result of the one-pass simulations, miniaturization of microchannel dimensions begins to limit effectiveness and power density as a result of axial conduction, pressure drop, and a temperature gradient forming within the channels. To reach high performance, a design change is required.

The final set of simulations tested an 8YSZ multi-pass heat exchanger system consisting of one-pass layers stacked on one another, with 36 total one pass layers per fluid. It utilizes a counterflow design as the hot and cold fluids start at opposite ends of the heat exchanger, while hot and cold layers are arranged in a crossflow pattern. Two different channel sizes were tested at 0.5 mm and 0.05 mm. Gas routing comes from an external manifold with two one-pass layers per pass. The flow rates varied from a Reynold's number of 200 to 5,000.

16) Both channel dimensions reached an effectiveness over 0.91 with the 0.05 mm channel experiencing a slightly decreased peak effectiveness, similar to that of one-pass systems.
17) The 0.05 mm channel dimension had a peak effectiveness of 3300 W/g, which exceeds the power density achieved using one-pass configurations. Both systems experienced a similar behavior of increased power density at higher flow rates.
18) Both heat exchangers experienced an identical drop off in effectiveness at high Reynold's numbers. However, both maintained an effectiveness over 0.9 for flow rates up to 1000 Re.
19) The multi-pass design achieved an 11.2 times increase in power density and 1.08 times increase in maximum achievable effectiveness over leading commercial heat exchanger designs.

REFERENCES

1. David C. Denkenberger, Michael J. Brandemuehl, Joshua M. Pearce, and John Zhai, "Expanded microchannel heat exchanger: design, fabrication and preliminary experimental test", Proceedings of the Institution of Mechanical Engineers – Part A: Journal of Power and Energy, 226, 532544 (2012). http://dx.doi.org/10.1177/0957650912442781

2. Brandner, JJ., Bohn, L., Hansjosten, E., Henning, T., Schygulla, U., Wenka, A., Schubert, K. "Concepts and Realization of Microstructure Heat Exchangers for Enhanced Heat Transfer." Experimental Thermal and Fluid Science 30, no. 8 (August 2006): 801-9. https://doi.org/10.1016/j.expthermflusci.2006.03.009

3. Kee, Robert J., Berkeley B. Almand, Justin M. Blasi, Benjamin L. Rosen, Marco Hartmann, Neal P. Sullivan, Huayang Zhu, et al. "The Design, Fabrication, and Evaluation of a Ceramic Counter-Flow Microchannel Heat Exchanger." Applied Thermal Engineering 31, no. 11–12 (August 2011): 2004–12. https://doi.org/10.1016/j.applthermaleng.2011.03.009.

4. Murphy, Danielle M., Anthony Manerbino, Margarite Parker, Justin Blasi, Robert J. Kee, and Neal P. Sullivan. "Methane Steam Reforming in a Novel Ceramic Microchannel Reactor." International Journal of Hydrogen Energy 38, no. 21 (July 2013): 8741–50. https://doi.org/10.1016/j.ijhydene.2013.05.014.

5. "Overview of Greenhouse Gases." EPA, April 13, 2023. https://www.epa.gov/ghgemissions/overview-greenhouse-gases.

6. Boldrin, Paul, and Nigel P. Brandon. "Progress and Outlook for Solid Oxide Fuel Cells for Transportation Applications." Nature Catalysis 2, no. 7 (July 11, 2019): 571–77. https://doi.org/10.1038/s41929-019-0310-y.

7. Sridhar, Kolepaka. "Comparative Analysis of Parallel and Counter Flow Heat Exchangers." International Journal of Scientific Engineering and Technology Research 6, no. 4 (February 2017): 638–44.

8. Harms, Todd M., Michael J. Kazmierczak, and Frank M. Gerner. "Developing Convective Heat Transfer in Deep Rectangular Microchannels." International Journal of Heat and Fluid Flow 20, no. 2 (April 1999): 149–57. https://doi.org/10.1016/s0142-727x(98)10055-3.

9. Lewinsohn, Charles. “High-Efficiency, Ceramic Microchannel Heat Exchangers.” American Ceramic Society Bulletin 94, no. 5 (2015).

10. Hasan, Mushtaq I., A.A. Rageb, M. Yaghoubi, and Homayon Homayoni. “Influence of Channel Geometry on the Performance of a Counter Flow Microchannel Heat Exchanger.” International Journal of Thermal Sciences 48, no. 8 (August 2009): 1607–18. https://doi.org/10.1016/j.ijthermalsci.2009.01.004.

11. Muzychka, Y.S. “Constructal Design of Forced Convection Cooled Microchannel Heat Sinks and Heat Exchangers.” International Journal of Heat and Mass Transfer 48, no. 15 (July 2005): 3119–27. https://doi.org/10.1016/j.ijheatmasstransfer.2005.02.014.

12. Kumar R, Avinash, Kavitha M, P Manoj Kumar, and Arvindh Seshadri S. “The Hydraulic and Thermal Performances of Rectangular and Square Microchannel with Different Hydraulic Diameters Cooled by Graphene–Platinum Hybrid Nanofluid.” Proceedings of the Institution of Mechanical Engineers, Part C: Journal of Mechanical Engineering Science 236, no. 13 (January 28, 2022): 7473–83. https://doi.org/10.1177/09544062211072706.

13. Vontas, Konstantinos, Manolia Andredaki, Anastasios Georgoulas, Nicolas Miché, and Marco Marengo. “The Effect of Hydraulic Diameter on Flow Boiling within Single Rectangular Microchannels and Comparison of Heat Sink Configuration of a Single and Multiple Microchannels.” Energies 14, no. 20 (October 14, 2021): 6641. https://doi.org/10.3390/en14206641.

14. Mortensen, Niels Asger, Fridolin Okkels, and Henrik Bruus. “Reexamination of Hagen-Poiseuille Flow: Shape Dependence of the Hydraulic Resistance in Microchannels.” Physical Review E 71, no. 5 (May 5, 2005). https://doi.org/10.1103/physreve.71.057301.

15. Maranzana, Gaël, Isabelle Perry, and Denis Maillet. “Mini- and Micro-Channels: Influence of Axial Conduction in the Walls.” International Journal of Heat and Mass Transfer 47, no. 17–18 (August 2004): 3993–4004. https://doi.org/10.1016/j.ijheatmasstransfer.2004.04.016.

16. Lo Faro, M., V. Antonucci, P.L. Antonucci, and A.S. Aricò. “Fuel Flexibility: A Key Challenge for SOFC Technology.” Fuel 102 (July 25, 2012): 554–59. https://doi.org/10.1016/j.fuel.2012.07.031.

17.Huber, Marcia L., and Allan H. Harvey. “Thermal Conductivity of Gases.” NIST, February 20, 2017. https://www.nist.gov/publications/thermal-conductivity-gases.

18. Huber, Marcia L., and Allan H. Harvey. “Viscosity of Gases.” NIST, February 20, 2017. https://www.nist.gov/publications/viscosity-gases.

19. Momma, Akihiko, Kiyonami Takano, Yohei Tanaka, Tohru Kato, and Atsushi Yamamoto. “Experimental Investigation of the Effect of Operating Pressure on the Performance of SOFC and SOEC.” ECS Transactions 57, no. 1 (2013): 699–708. https://doi.org/10.1149/05701.0699ecst.

20. Brett, Daniel J., Alan Atkinson, Nigel P. Brandon, and Stephen J. Skinner. “Intermediate Temperature Solid Oxide Fuel Cells.” Chemical Society Reviews 37, no. 8 (May 28, 2008): 1568–78. https://doi.org/10.1039/b612060c.

21. Zarabi Golkhatmi, Sanaz, Muhammad Imran Asghar, and Peter D. Lund. “A Review on Solid Oxide Fuel Cell Durability: Latest Progress, Mechanisms, and Study Tools.” Renewable and Sustainable Energy Reviews 161 (March 9, 2022): 112339. https://doi.org/10.1016/j.rser.2022.112339.

22. Yokokawa, Harumi, Hengyong Tu, Boris Iwanschitz, and Andreas Mai. “Fundamental Mechanisms Limiting Solid Oxide Fuel Cell Durability.” Journal of Power Sources 182, no. 2 (August 1, 2008): 400–412. https://doi.org/10.1016/j.jpowsour.2008.02.016.

23. Dokiya, Masayaki. “SOFC System and Technology.” Solid State Ionics 152-153 (December 2022): 383-92. https://doi.org/10.1016/S0167-2738(02)00345-4

24. Xu, Qidong, Zengjia Guo, Lingchao Xia, Qijiao He, Zheng Li, Idris Temitope Bello, Keqing Zheng, and Meng Ni. “A Comprehensive Review of Solid Oxide Fuel Cells Operating on Various Promising Alternative Fuels.” Energy Conversion and Management 253 (February 1, 2022). https://doi.org/10.1016/j.enconman.2021.115175.

25. Wang, Yi, Wenyuan Li, Liang Ma, Wei Li, and Xingbo Liu. “Degradation of Solid Oxide Electrolysis Cells: Phenomena, Mechanisms, and Emerging Mitigation Strategies—A Review.” Journal of Materials Science & Technology 55 (October 15, 2020): 35–55. https://doi.org/10.1016/j.jmst.2019.07.026.

26. Williams, Mike, Arun Muley, Jim Bolla, and Hal Strumpf. “Advanced Heat Exchanger Technology for Aerospace Applications.” SAE Technical Paper Series, November 2008. https://doi.org/10.4271/2008-01-2903.

27. Mei, Fanghua, Pritish R Parida, Jing Jiang, Wen Jin Meng, and Srinath Wen Jin Ekkad. “Fabrication, Assembly, and Testing of Cu- and al-Based Microchannel Heat Exchangers.” Journal of Microelectromechanical Systems 17, no. 4 (August 2008): 869–81. https://doi.org/10.1109/jmems.2008.924276.

28. Khan, Mesbah G., and Amir Fartaj. “A Review on Microchannel Heat Exchangers and Potential Applications.” International Journal of Energy Research 35, no. 7 (May 6, 2011): 553–82. https://doi.org/10.1002/er.1720.

29. Jiang, San Ping. “Challenges in the Development of Reversible Solid Oxide Cell Technologies: A Mini Review.” Asia-Pacific Journal of Chemical Engineering 11, no. 3 (March 29, 2016): 386–91. https://doi.org/10.1002/apj.1987.

30. Alm, B, U Imke, R Knitter, U Schygulla, and S Zimmermann. “Testing and Simulation of Ceramic Micro Heat Exchangers.” Chemical Engineering Journal 135 (January 15, 2008). https://doi.org/10.1016/j.cej.2007.07.005.

31. Kaur, Inderjot, and Prashant Singh. “State-of-the-Art in Heat Exchanger Additive Manufacturing.” International Journal of Heat and Mass Transfer 178 (October 2021). https://doi.org/10.1016/j.ijheatmasstransfer.2021.121600.

32. Yih, James, and Hailei Wang. “Experimental Characterization of Thermal-Hydraulic Performance of a Microchannel Heat Exchanger for Waste Heat Recovery.” Energy Conversion and Management 204 (January 15, 2020): 112309. https://doi.org/10.1016/j.enconman.2019.112309.

33. Tiwari, Ratnesh, Rohit S. Andhare, Amir Shooshtari, and Michael Ohadi. “Development of an Additive Manufacturing-Enabled Compact Manifold Microchannel Heat Exchanger.” Applied Thermal Engineering 147 (January 25, 2019): 781–88. https://doi.org/10.1016/j.applthermaleng.2018.10.122.

34. Matsson, John E. An introduction to solidworks® flow simulation 2021. Mission, KS: SDC Publications, 2021.

35. Technical Reference SolidWorks Flow Simulation 2021. Dassault Systems, 2020.

36. Zhou, Fang, Weisong Ling, Wei Zhou, Qingfu Qiu, and Xuyang Chu. “Heat Transfer Characteristics of Cu-Based Microchannel Heat Exchanger Fabricated by Multi-Blade Milling Process.” International Journal of Thermal Sciences 138 (April 2019): 559–75. https://doi.org/10.1016/j.ijthermalsci.2019.01.007.

37. Erdoğan, Meryem, and C. Imrak. “The Effects of Duct Shape on the Nusselt Number.” Mathematical and Computational Applications 10, no. 1 (2005): 79–88. https://doi.org/10.3390/mca10010079.

38. Parahovnik, Anatoly, Nir Tzabar, Yotam Haas, Lora Parahovnik, Israel Rosinsky, and Gilad Yossifon. “Evaluation of Axial Conduction Effects and Heat Losses in Counter-Flow Microscale Heat Exchangers.” Applied Thermal Engineering 121 (July 5, 2017): 1095–1101. https://doi.org/10.1016/j.applthermaleng.2017.04.052.

39. Jacobson, Allan J. “Materials for Solid Oxide Fuel Cells.” Chemistry of Materials 22, no. 3 (November 20, 2009): 660–74. https://doi.org/10.1021/cm902640j.

40. Zamudio-García, Javier, Leire Caizán-Juanarena, José M. Porras-Vázquez, Enrique R. Losilla, and David Marrero-López. “A Review on Recent Advances and Trends in Symmetrical Electrodes for Solid Oxide Cells.” Journal of Power Sources 520 (February 1, 2022). https://doi.org/10.1016/j.jpowsour.2021.230852.

APPENDIX

APPENDIX A: NOMENCLATURE

A: Area

A_s: Surface Area

℃: Celcius

CH_4: Methane Gas

C_{min}: Heat capacity rate of cold fluid

C_{max}: Heat capacity rate of hot fluid

$C_{p,C}$: Specific heat of cold fluid

$C_{p,H}$: Specific heat of hot fluid

D_h: Hydraulic Diameter

e: Exponential

g: Gram

H_2: Hydrogen Gas

$h_{C,i}$: Cold inlet enthalpy

$h_{C,o}$: Cold outlet enthalpy

$h_{H,i}$: Hot inlet enthalpy

$\dot{h}_{C,i}$: Cold inlet enthalpy rate

$\dot{h}_{C,o}$: Cold outlet enthalpy rate

$\dot{h}_{H,i}$: Hot inlet enthalpy rate

h: Convective heat transfer coefficient

K: Kelvin

k: Thermal conductivity of solid material

k_{Fluid}: Thermal conductivity of fluid

kg: Kilogram

L: Length

m: Meter

m^3: Cubic meter

mm: Millimeter

$\dot{m}_C$: Cold mass flow rate

$\dot{m}_H$: Hot mass flow rate

Nu: Nusselt number

NTU: Number of transfer units

O_2: Oxygen gas

P: Power Density

Q: Volumetric flow rate

R: Ratio of thermal capacities

R_{Cond}: Conductive thermal resistance

$R_{Conv,C}$: Convective thermal resistance for cold fluid

$R_{Conv,H}$: Convective thermal resistance for hot fluid

Re: Reynold's number

R_{Th}: Thermal resistance

s: Seconds

$T_{C,i}$: Cold inlet temperature

$T_{C,o}$: Cold outlet temperature

$T_{H,i}$: Hot inlet temperature

U: Overall heat transfer coefficient

V: Volume

W: Watts

Greek Letters

ε: Effectiveness

μm: Micrometer

μPa: Micropascal

π: Pi

ρ: Density

ΔP: Pressure Drop